#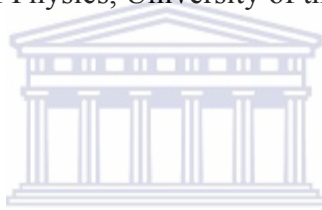 FABRICATION AND CHARACTERIZATION OF A SOLAR CELL USING AN ALUMINIUM P-DOPED LAYER IN THE HOT-WIRE CHEMICAL VAPOUR DEPOSITION PROCESS

Kotsedi Lebogang

A thesis submitted in partial fulfillment of the requirements for the degree of Doctor Philosophiae in the Department of Physics, University of the Western Cape.

Promoter: Prof. D. Knoesen
Co-Promoter: Prof. R Madjoe

June 2010.

i

Keywords

Hot-Wire Chemical Vapour Deposition

Aluminium

Doping

Hydrogenated amorphous silicon

Phosphine

Solar cell

Photovoltaic

Nanocrystalline

Thin Film

Indium Tin Oxide

Abstract

When the amorphous silicon (a-Si) dangling bonds are bonded to hydrogen the concentration of the dangling bond is decreased. The resulting film is called hydrogenated amorphous silicon (a-Si:H). The reduction in the dangling bonds concentration improves the opto-electrical properties of the film. The improved properties of a-Si:H makes it possible to manufacture electronic devices including a solar cell.

A solar cell device based on the hydrogenated amorphous silicon (a-Si:H) was fabricated using the Hot-Wire Chemical Vapour Deposition (HWCVD). When an n-i-p solar cell configuration is grown, the norm is that the p-doped layer is deposited from a mixture of silane (SiH_4) gas with diborane (B_2H_6). The boron atoms from diborane bonds to the silicon atoms and because of the number of the valance electrons, the grown film becomes a p-type film. Aluminium is a group 3B element and has the same valence electrons as boron, hence it will also produce a p-type film when it bonds with silicon.

In this study the p-doped layer is grown from the co-deposition of a-Si:H from SiH_4 with aluminium evaporation resulting in a crystallized, p-doped thin film. When this thin film is used in the n-i-p cell configuration, the device shows photo-voltaic activity.

The intrinsic layer and the n-type layers for the solar cell were grown from SiH_4 gas and Phosphine (PH_3) gas diluted in SiH_4 respectively. The individual layers of the solar cell device were characterized for both their optical and electrical properties. This was done using a variety of experimental techniques. The analyzed results from the characterization techniques showed the films to be of device quality standard. The analysed results of the p-type layer grown from aluminium showed the film to be successfully crystallized and doped.

A fully functional solar cell was fabricated from these layers and the cell showed photovoltaic activity.

DECLARATION

I declare that the study of "Fabrication and characterization of solar cell using the aluminium p-doped layer in the Hot-Wire Chemical Vapour Deposition (HWCVD)" is my own work, that it has not been submitted for any degree or examination in any other university, and that all the sources I have used or quoted have been indicated and acknowledged by complete references.

Lebogang Kotsedi

Signed:

Date:

ACKNOWLEDGEMENTS

Content

Chapter 1 : INTRODUCTION

Chapter 2 : EXPERIMENTAL METHODS

Chapter : 3 RESULTS AND DISCUSSION

CHAPTER 4 DOPING

CHAPTER 5

Chapter 1

Introduction

1.1 Renewable energy

The climate of the earth has it own natural cycle, in that the earth and its atmosphere go through changes in temperature to accommodate the change in the amount of energy received from the sun. These variations in the climate's natural cycle have resulted in warm and cold periods [1.1].

There is a well founded concern, that it is human intervention (for example, industrialization) that is causing the climate to change at an alarming un-natural rate. This is a consequence of the large amount of the green house gases that are being released by human activities into the atmosphere. Burning of fossil fuel (oil, coal and natural gases) as a means of generating electricity is one of the major contributors of green house gas emissions [1.2]. These green house gases trap the infrared radiation from the sun within the earth's atmosphere, causing the earth temperature to increase faster than the natural cycle of the earth's climate.

In South Africa it is predicted that the mean air temperature will increase by approximately 2 $^{\circ}$C over the next century [1.2]. These facts demand alternative ways of producing energy (electrical), as well as a review of our industrial processes amongst other things.

There are several natural options that the earth provides as possible resources for the production of electricity from its renewable sources, like wind energy, geothermal, tidal and *solar energy* which are environmentally benign and do not tamper with the earth's natural climate. South Africa has realized the pressing need of these alternative energy technologies and has signed the 'Washington Declaration' in 2007 [1.3].

This is an agreement on the principles of the Kyoto protocol (United Nations framework on climate change held in Brazil June 1992).

1.2 Solar energy

The radiation energy of the sun on the earth is about 1.5×10^{18} kWh per year [1.4], this radiation energy from the sun peaks at wavelengths between 200 nm to 3000 nm in the electromagnetic spectrum [1.5].

This energy from the sun can be converted to clean electricity by using photovoltaic materials or solar cells. These are solid state materials that absorb photon energy from the sun and convert it to a usable 'green' electrical energy. This method of renewable energy has gained much interest in recent decades, due to its ability to be accessed by the population because it can easily be installed in their houses, especially in remote areas.

During the past two decades an economic way of manufacturing these solar cells has emerged by using hydrogenated amorphous silicon (a-Si:H) thin films technology. This method has garnered much interest in the field of photovoltaic research because of its low cost of manufacturing, due to the fact that this material has a high absorption coefficient [1.6], hence only thin films of a-Si:H are needed to successfully induce meaningful photovoltaic activity. The other advantage a-Si:H has is that it can be grown on large surface areas and flexible materials [1.7]. There is also a wide scope for research in improving the technology of the hydrogenated amorphous silicon.

1.3 Hydrogenated amorphous silicon (a-Si:H)

An amorphous material usually has a short range order structure, this is due to the absence of long range repetitive unit cell structures. This is because of the fluctuations in the bond lengths and bond angles during the growth of the amorphous materials [1.8].

In *amorphous silicon* (a-Si), a silicon atom has a four fold covalent bonding with its neighbouring atoms, but this is true only for a short range [1.8,1.9]. As the atoms coalesce and conglomerate during the growth of the film, the bonding angles distort and the bond lengths fluctuate. The results of this effect are dangling (unsatisfied) silicon bonds in the growing material. The absence of long range periodicity in *amorphous silicon* (a-Si) makes the concept of conservation of momentum undefined, this causes the optical processes in this class of material (amorphous silicon) to show direct band gap behaviour [1.10]. This phenomenon causes the amorphous silicon to have a greater optical absorption coefficient (α), that is because the optical absorption coefficient is determined by the availability of the electronic state only. Amorphous silicon (a-Si) has a greater optical absorption (α) in the visible region of the spectrum as compared to single crystalline silicon.

The fluctuations in bond angles and bond lengths introduce band tails in the density of electronic states, from both the conduction and the valence bands into the band gap, in combination with defect states in the band gap of the material [1.8]. These physical variations in the a-Si have detrimental effects on the electronic properties of the a-Si for solar cell application. The dangling bonds in a-Si also have a detrimental role in the opto-electronic properties of the amorphous silicon [1.11].

The dangling bonds concentration in the a-Si can be reduced by bonding them with hydrogen atoms. This has improve the electronic properties of a-Si [1.12]. When hydrogen is incorporated in the amorphous silicon network it reduces the band tail densities in the growing material, this happens as the hydrogen satisfies the dangling bonds in amorphous silicon [1.8]. The resulting material is known as *hydrogenated amorphous silicon* (a-Si:H). The order of magnitude in which the dangling bonds can be reduced depends on the deposition conditions used to grow the film. This process of bonding hydrogen to the dangling bonds makes it possible to manufacture device quality *hydrogenated amorphous silicon* (a-Si:H) films. The grown films can be used for solar

cell application. Silane (SiH_4) gas is a common precursor used in the deposition of a device quality a-Si:H film [1.8].

Thin films of a-Si:H can be grown using either the Plasma Enhanced Chemical Vapour Deposition (PECVD), or the Hot Wire Chemical Vapour Deposition (HWCVD) techniques. These are the most popular deposition techniques amongst other techniques in the field of a-Si:H film [1.13].

In the PECVD technique thin films of a-Si:H are grown on a heated substrate, the deposition happens when silane molecules interact with the plasma of electrons in an evacuated reaction chamber. The plasma of electrons split the silane gas into silicon and hydrogen ions. The plasma of electrons is maintained by the electric field between two parallel plates in the reaction chamber. This can be achieved using either dc voltage or ac voltage in the radio frequency domain (13.65 – 200 MHz) [1.14]. The interaction of silane with the plasma of electrons results in the generation of positive and negative ions, radicals and electrons in the reaction chamber. The growth of device quality a-Si:H film using the PECVD is dependent on the rf power, the frequency, the electrode geometry, and the geometry of the vacuum chamber.

In the Hot Wire Chemical Vapour Deposition (HWCVD) technique silane gas pyro-catalytically interacts with the resistively heated wire [1.15]. The heated wire in this study was a tantalum wire. The tantalum wire is heated to temperatures where the tungsten-silicide formation on the wire is avoided [1.16]. When the silane molecules interact with the heated wire they fragment into silicon and hydrogen radicals. On their way to the heated substrate these radicals react at varying stochiometry depending on the deposition parameters.

 Different microstructures of device quality films can be grown using the HWCVD technique, this can be achieved by changing only a few parameters without even opening

4

the reaction chamber. The absence of an electron plasma in the reaction chamber saves the growing film from damage by the electrons from the plasma. HWCVD is also known for its higher deposition rate of device quality films [1.13].

1.4 Doping

The first doping of the a-Si:H was reported by Spears and LeComber in 1975, this was achieved by diluting SiH_4 with Phosphine (PH_3) for n-type doping and Diborane (BH_3) for p-type doping during growth of doped a-Si:H thin films [1.17]. From the periodic chart of elements it is observed that boron is a group 3B element and phosphorous is a group 5B element. It is known that when group 3B elements are incorporated in a silicon (Si) atomic network of a-Si:H thin film for the purposes of doping they give p-type material, in the same way a group 5B element will result in n-type doped material when incorporated into the a-Si:H film [1.8].

Phosphine (PH_3) diluted in silane (SiH_4) gas is used to incorporate phosphorous ions to bond with silicon (Si) atoms in the a-Si:H film network, during the growth of a-SiP:H thin film resulting in an n-type doped film. The same happens when diborane gas is diluted in silane, boron atoms bond with silicon atoms in a-Si:H resulting in the a-SiB:H network which is p-type.

Aluminium is also a group 3B element, and it is also known to have an effect (known as aluminium induced crystallization (AIC)) of crystallizing a-Si:H films. The AIC process requires that the aluminium layer be evaporated onto a-Si:H film [1.18]. In some cases a-Si:H film is grown onto a substrate that has aluminium evaporated on it [1.19,1.20]. To activate the crystallization of a-Si:H, the sample has to be annealed at elevated temperatures. A meaningful crystallization normally begins to happen after a short period when the furnace temperature is around 450 ^{o}C [1.21].

To have crystallization taking place throughout the bulk of a-Si:H film, the sample has to be annealed for longer periods.

Recently this process of aluminium induced crystallization (AIC) was used to grow a p-type layer in the manufacturing of a fully functional solar cell [1.22]. This proves that aluminium can be used for p-type doping of a-Si:H by virtue of its position as a group 3B element.

A new and faster method of crystallizing and p-doping a-Si:H will be introduced in this study. Instead of annealing a-Si:H film covered with aluminium, a single step growth process will be done in a HWCVD chamber. In this new method aluminium will be evaporated in the HWCVD chamber, the evaporated aluminium will react with silicon and hydrogen atoms from the fragmented silane. The end product of this process will be a p-doped, crystallized film on a substrate. The crystallization in the grown film will be throughout the bulk of the film, also the films won't need any post-deposition annealing to activate crystallization. In this novel process, aluminium induced crystallized p-doped (**AICPD**) films will be grown on a substrate of choice using the HWCVD technique via just a single step process reaction.

1.5 Solar Cell

The first functional a-Si:H solar cell was reported by Carlson and Wronski [1.23], a-Si:H solar cells are normally made from the thin film of an intrinsic (i) layer sandwiched between thin layers of p- and n-type doped a-Si:H. The intrinsic layer is the part of the cell that absorbs most of the incident photon energy [1.13].This photon energy is used to photo-excite the active charge carriers from the valence band to the conduction band. In the process there are holes created in the valence band equaling the number of electrons that are excited to the conduction band. The electric field created by the doped layers

cause holes and electrons in the (i) layer to drift. The drift current is the dominant mechanism for the flow of charges, and this is due to the high levels of defect densities in amorphous materials causing a small diffusion length, typically 200 nm [1.4].

1.6 Deposition

a-Si:H thin films can be deposited using various methods, but recently the Hot Wire Chemical Vapour Deposition (HWCVD) method has gained popularity in the a-Si:H field. It is because of the fast deposition rate and good quality intrinsic thin films with low hydrogen concentration which makes this deposition technique attract more research interest [1.13].

a-Si:H thin films are deposited on a substrate of choice using silane (SiH_4) gas as a precursor. When silane gas collides with a resistively heated hot tantalum wire it pyrolytically decomposes into silicon and hydrogen atoms. The silicon and hydrogen atoms reacts on their way to the heated substrate forming SiH_x (x = 1, 2 or 3) radicals depending on the deposition conditions [1.24]. These silicon hydrides radicals then agglomerate and coalesce on the heated substrate and grow to form an a-Si:H thin film [1.25]. The same process occurs when the dopant gases (PH_3 and BH_3) are diluted in silane to grow n- and p-type thin films.

Aim and Outline

The HWCVD has been developing over the years and technological device quality thin films have been grown using this technique. Both intrinsic and doped films of a-Si:H can be grown by the HWCVD technique for solar cell application.

The aim of this study is to build a fully functional solar cell using the HWCVD technique. The device configuration that is intended for this work is a n-i-p structure.

The p-layer of this device will be grown my doping the amorphous silicon with aluminium in a novel process called AICPD. In this configuration the n-type layer is the window layer. The intrinsic layer is the active layer where the photo-excited carriers are generated. The p-type layer in this cell in conjunction with the n-type layer creates an electric field and this field drifts the charged carrier in the intrinsic layer, resulting in the generation of electric current.

In chapter two HWCVD parameters employed in the deposition processes will be looked at in detail, and that will be followed by a comprehensive background of the experimental methods used to analyse all the films.

Chapter three will focus on the deposition parameters chosen for the growth of the intrinsic layer. Then a detailed discussion of the analytical results of this film will be presented. A summary of the structural and optical analysis will be tabulated at the end of this chapter.

Chapter four will be a section where the analytical results of n-type and p-type layers will presented. The n-type layer structural results and optical results will be discussed in this section, those results will be followed by electrical characterization. An overview of the n-type analytical results will be tabulated at the end of the section. The structural and electrical results of the grown p-type from the process of aluminium induced crystallized p-doped (**AICPD**) film will also be discussed.
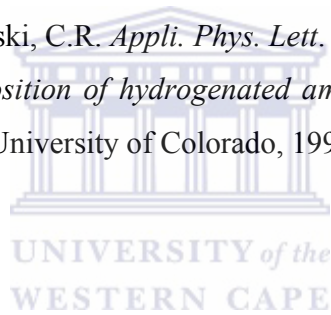
Chapter five will deal with the fabrication of a fully functional solar cell that uses aluminium induced crystallized p-doped (**AICPD**) film. A brief comparison of the open circuit voltage (V_{oc}) and short circuit current (J_{sc}) will done. This will be from cells grown from varying deposition conditions. Conclusion and recommendations will be stated at the end of the chapter.

1. 8 References:

[1.1] Houghton, John Theodore, ed (2001). *Climate change 2001: the scientific basis: contribution of Working Group I to the Third Assessment Report of the Intergovernmental Panel on Climate Change*. Cambridge, UK: Cambridge University Press. ISBN 0-521-80767-0.

[1.2] A National Climate Response Strategy For South Africa, September 2004, Deparment of Environmental Affairs and Tourism. ISBN # 0-7803-1460-3

[1.3] http://www.ituc-csi.org/IMG/pdf/0811t_gf_G20.pdf

[1.4] K.F. Feenstra, *Hot-wire chemical vapour deposition of amorphous silicon and the application in solar cells*, Ph.D thesis, Utrecht University , 1998.

[1.5] S.M. Sze, in Semiconductor Devices, John Wiley & Sons, New York (1985)

[1.6] Progress in PHOTOVOTAICS: Research and Application, Volume 6, Issue 3 page 181 -186 (1998).

[1.7] Photovoltaic Energy Conversion, 1994., Conference Record of the Twenty Fourth. IEEE Photovoltaic Specialists Conference - IEEE First World Conference 1994.

[1.8] R.A. Street*, Hydrogenated amorphous silicon,* Cambridge University Press (1991).

[1.9] W.E. Spear, Proceedings Royal Society London **A 420,** 201 - 218 (1988).

[1.10] J. Tauc, Optical Properties of Solids, edited by F. Abeles (North-Holland, Amsterdam, the Netherlands) (1972)

[1.11] N.F. Mott, E.A. Davis Electronic Processes in Non-crystalline materials, Clarendon Press, Oxford, U.K. (1971)

[1.12] A.J. Lewis, G.A.N. Connell, W. Paul, J. Pawlik, R. Temkin, AIP Conference. Proceedings. **20**, 27 (1974)

 [1.13] R.E.I. Schropp and M. Zeman, *Amorphous and microcrystalline silicon solar cell: Modeling, Materials and Device Technology*, Kluwer Academic Publisher (1998).

[1.14] H. Meiling, *Deposition of amorphous thin film and solar cells*, Ph.D. Thesis (Utrecht University, (1991)

[1.15] H.A. Mahan, B.P. Nelson, S. Salamon, R.S. Crandall, Journal of Non-Crystalline Solids **137 & 138** 657-660 (1991).

[1.16] P.A.T.T. van Veenendaal., Ph.D thesis, Utrecht University, (1998)

References:

[1.17] Spear, W.E. and LeComber, P.G. Solid State Comm. **17**, 1193 (1975).

[1.18] O. Nast, T. Puzzer, L. M. Koschier, A. B. Sproul, and S. R. Wenham, Appl. Phys. Lett. **73**, 3214 (1998).

[1.19] O. Nast, S.R. Wenham, J. Appl. Phys. **88** 124 (2000)

[1.20] O. Nast, Hartmann, J. Appl. Phys. **88** 716 (2000)

[1.21] J. Schneider, J. Klein, M. Muske, S. Gall, E. Fuhs. J. Non-Cryst. Solids. **338 -340** 127 – 130 (2004).

[1.22] S.Gall, J.Schneider, K. Hubener, M. Muske, B. Rau, E. Conrad, I. Sieber, K. Petter, K. Lips, M. Stoger-Pollach, P Schattschneider, W Fuhs, *Thin Solid Films* **511 – 512** 7 – 14 (2006).

[1.23] Carlson, D.E. and Wronski, C.R. *Appli. Phys. Lett*. **28**, 671 (1976).

[1.24] E.C. Molenbroek*, Deposition of hydrogenated amorphous silicon with the hot – wire technique* (P.hD. Thesis, University of Colorado, 1995)

Chapter 2

Experimental methods

2.1 The Hot Wire Chemical Vapour Deposition (HWCVD)

2.1.1 Introduction

The Hot Wire Chemical Vapour Deposition process is a technique that is used to grow thin films of a-Si:H, these films can be grown either intrinsic or doped on a substrate of choice. In this process a resistively heated tantalum wire is used to crack the precursor gases into their constituent atoms when they pyro-catalytically interact with the hot tantalum wire [2.1,2.2]. The process is shown schematically in figure 2.1.

Silane

Hydrogen

Silicon atom

Figure 2.1. A schematic diagram of the HWCVD chamber.

In the HWCVD process a thin film of a-Si:H is grown by introducing a precursor gas into the reaction chamber that is under high vacuum. For this study silane gas was used as the precursor gas of choice for growing thin films of a-Si:H. The flow rate of the gas from the feedstock to the reaction chamber is carefully controlled by the mass flow controllers. The precursor gas is then sprayed into the reaction chamber through the gas shower inlet parallel to the heated tantalum wire. When the silane interacts with the hot tantalum wire it fragments into silicon and hydrogen atoms [2.1-2.3].

On their way to the heated substrate, the hydrogen and silicon atoms react with each other. The reactions happen in varying stoichiometry depending on the values of the deposition parameters [2.2]. These deposition parameters also have an effect on the reactions of the species on the heated substrate during the growth of the film. At an 'optimum deposition' regime there are desirable secondary gas phase reactions which includes hydrogen radicals reacting with silane forming SiH_3 species in the gas phase reactions [2.4].

When these silicon hydride molecules come into contact with the heated substrate they start to migrate on the surface till they find suitable sites. During this process there exists a probability that some of the silicon hydrate species might be desorbed from the substrate, and those that survive stick to the substrate. These adsorbed species then agglomerate and coalesce to form an a-Si:H thin film [2.5]. In this process of thin film growth, hydrogen atoms bond to the weak unsaturated silicon bonds to saturate them, this prevents them partaking in any further chemical activities and resulting in a film with fewer dangling bonds [2.6].

2.2 Deposition conditions

The quality of the deposited film is largely dependent on the values of the deposition parameters that were used during the growth of the a-Si:H. There are several variables in

the HWCVD process that plays a role in the quality of the deposited a-Si:H film. The 'optimum regime' of this variable during deposition will give a device quality a-Si:H film.

2.2.1 Deposition parameters in the HWCD chamber

The growth of a thin film in the HWCVD reaction chamber is dependant on a set of technological parameters in the HWCVD process. These technological parameters are the deposition *pressure* in the reaction chamber, *the flow rate* and *the gas ratios* of the precursor gases into the reaction chamber, *the substrate to filament distance*, the *substrate temperature* and the *filament temperature*.

The deposition *pressure* during the growth of a-Si:H film plays a pivotal role. The structure and opto-electrical properties of the resulting film is dependent on this parameter. The pressure in the chamber has a direct influence on the mean free path of the decomposed species, and the nature of the secondary gas phase reactions on their way to the heated substrate. Figure 2.2 figure shows the reaction of the radical in the chamber.
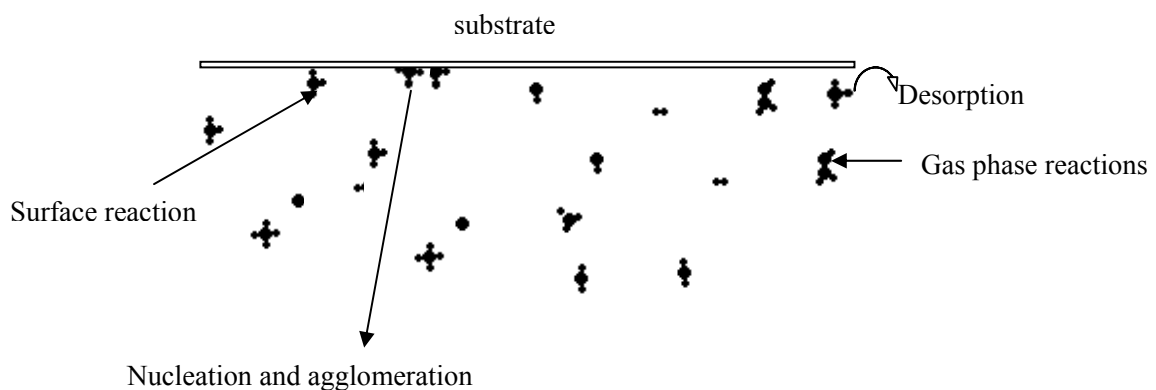

Figure 2.2. Schematic of the events that take place during the deposition of a a-Si:H film.

At higher deposition pressures than the optimum pressure, there are undesirable secondary gas phase polymerization reactions that result into a film with poor quality [2.7]. On the other hand when the operational pressure is lower than the optimum pressure, the film will suffer from a high flux of silicon atoms arriving on a substrate resulting in a film which is microvoid rich and has very pronounced microstructure factors [2.1]. The operational pressure should be chosen such that there are moderate amounts of secondary reactions, that will produce a film with good optoelectronic properties. The value of the operational pressure is also known to have a direct influence on the deposition rate of the a-Si:H film [2.7]. The greater the operational pressure, the higher the deposition rate of the film grown from the precursor gas. The operational pressure in the reaction chamber is kept constant at a pre-set value by a butterfly valve, this works in conjunction with the pressure sensor in the chamber.

The SiH_4 gas is introduced into the reaction chamber through the mass flow controller that is used to control the flow rate of the gases. The *flow rate* of the precursor gas plays a significant role in the end product during the growth of the a-Si:H film. The optimal flow rate is achieved when there is sufficient silane in the environment near the hot tantalum wire for pyro-catalytic reactions, and also enough to prevent the depletion of precursor gases in the reaction chamber for film growth [2.8]. The molecular weight of the precursor gas also has an influence on the operating pressure in the chamber. The heavier molecules will produce higher partial pressures than lighter molecules at the same flow rate into the reaction chamber.

The *filament-to-substrate distance* has shown to be an important parameter in the HWCVD processes. In the early stages of the development of this technique the quality of the grown film was not of device quality standard. One of the reasons for this was the non-optimum filament to substrate distance [2.1]. This parameter is pivotal in controlling

the range of the secondary reactions of the decomposed species on their way to the heated substrate. If this parameter falls outside of the optimum regime, the resulting film has poor optoelectronic quality and may result in an undesired atomic structure in the grown film. A *filament-to-substrate distance* that is too small will have a detrimental effect on the growing film, the heated filament will supply excessive heat radiation that may anneal the surface of the film, and this may lead to false readings of the substrate temperature.

Substrate temperature plays an important role in the quality of the grown a-Si:H film. This is because when the silicon hydride radicals arrive on the heated substrate, they start to migrate on the surface till they find suitable sites. For the growth of a good quality a-Si:H film, the substrate temperature needs to be high enough to allow sufficient mobility of the species on the substrate as they agglomerate and coalescence to form a thin film. At low substrate temperatures the diffusion coefficient is too low to allow structural equilibrium to be reached in the film. At too high temperatures most of the hydrogen does not remain an the grown film to help passivate dangling bonds, hence an optimum substrate temperature for deposition is desired [2.6].

For a good pyro-catalytic decomposition of precursor gases, the *filament temperature* must be above 1500 ^{o}C. If the tantalum filament temperature is below this value it usually results in the formation of silicides on the surface of the wire [2.5, 2.9] and this effect will reduce the catalytic ability of the hot wire and its life time. Similarly higher filament temperatures result in the tantalum evaporating, and that will lead to it being incorporated into the growing film resulting in a contaminated film that is less than device quality [2.9]. A filament temperature is chosen such that the two extremes are avoided during the film deposition.

It must be born in mind that all these parameters are inter-linked, the flow rate of the precursor gas set on the mass flow controller has an effect on the partial pressure, and temperature of the tantalum wire also has an effect on the pressure, this

is because the number of interactions of the molecules with the wire is proportional to the partial pressure of the species in the reaction chamber [2.10]. Hence all these deposition parameters are all interlinked and a fine balance between all these parameters must be maintained to grow a good technological a-Si:H film.

2.3 X-Ray Diffraction (XRD)

2.3.1 Introduction

X-rays are part of the electromagnetic radiation which has wavelengths in the range of 0.06 Å to 125 Å. The short wavelengths of the x-rays make them good probes for studying the atomic arrangement of crystallographic materials. The diffracted x-rays can be used to give information as to whether the sample that is being analyzed is either single crystalline, polycrystalline, microcrystalline or amorphous in their structural arrangement. Although for thin films the interaction volume for x-rays is very small, sufficient atomic interactions occur for a crystallographic analysis. When the sample that is being analyzed has any crystallinity in it, the XRD technique can give the crystallographic orientation of the atomic planes in the sample. The information of the atomic structure in the sample is extracted from the diffraction peaks on a XRD spectrum of the sample being analyzed. These peaks are indexed to give the orientations of the atomic planes in the sample using the PDF diffraction data base.

The $CuK\alpha_1$ x-ray radiation was used to study the microstructure of all the grown films. This x-ray radiation is produced when a thermionic gun capable of emitting electrons is heated by passing an electric current through it, and the emitted electrons are then accelerated through a potential difference of several kilovolts. When these accelerated electrons hit the copper metal target, some of the electrons from the copper metal are excited to the anti-bonding states from their orbitals. During this process electrons from

higher energy orbitals make transitions to fill the vacancies of the excited electrons. During this transition the energy difference between the initial and the final energy states is released in the form of an x-ray [2.11].

In the process of x-ray emission, x-rays of different wavelengths are emitted from the target material, but for the purpose of studying the atomic structure in the a-Si:H thin films a monochromatic x-ray radiation is needed. A filter material designed in such a way that the absorption edge which lies more towards the K_β wavelength of the copper target metal is used to filter off unwanted wavelengths.

These monochromatic x-rays from the x-ray tube impinge on the samples to be studied. In the process some x-rays are transmitted while some are diffracted by the atomic planes in the sample. The diffracted x-rays are collected by the detector and sorted by the digital data acquisition system. The crystallographic information of the sample under study is presented in the form of a XRD spectrum showing crystalline diffraction peaks or a hump in the case of amorphous materials [2.11, 2.12].

The θ - 2θ D8 Advanced Bruker XRD machine at iThemba LABS at Faure was used to study the microstructure of all the grown thin films.

2.3.2 XRD on amorphous material

From the Bragg condition, constructive interference takes place when the wavelengths of x-ray radiation have the same order or are multiple integers of the path between the scattering centers. The condition is satisfied when:

$$n\lambda = 2d \sin\theta \qquad (2.1)$$

Where

$n = 1,2,3,……$

λ - X-ray wavelength

d - Inter-plane distance

θ - Incident angle to the plane.

For the case of amorphous material it is known to exhibit a lack of long range order. The reason for this is the absence of a repetitive periodic unit cell structure. The Bragg condition cannot be satisfied in this class of materials, therefore a typical XRD spectrum for a-Si:H film as shown in figure 2.3 display a characteristic hump that is centered around ~28 $^{\text{o}}$. This hump is a characteristic feature of the amorphous material. The absence of diffraction peaks on the spectrum is due to the absence of constructive interference by the scattering centers.
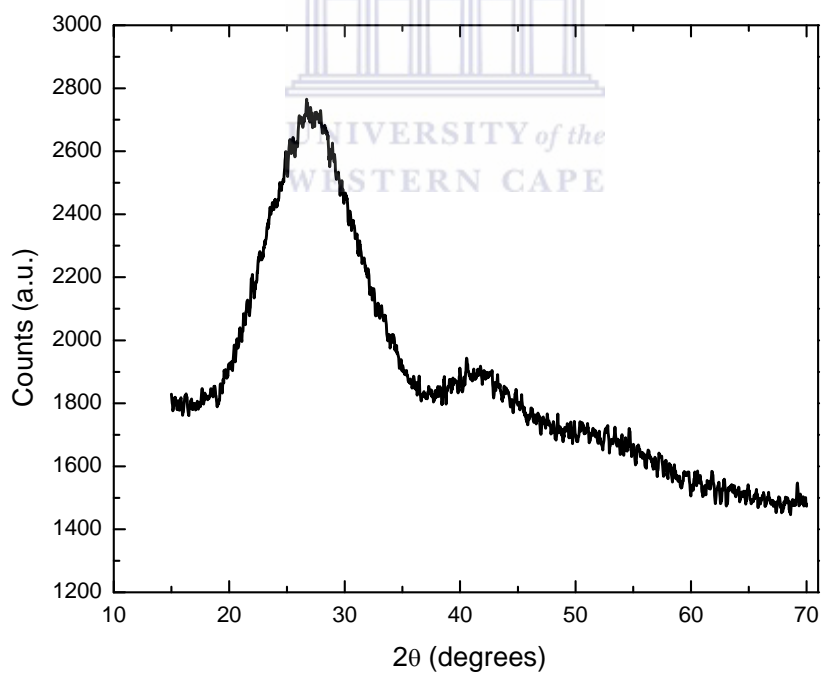

Figure 2.3. An XRD spectrometry spectrum of a-Si:H thin film on glass.

2.4 Optical parameters

2.4.1 Introduction

One of the unique features of a-Si:H is its optical constants and optoelectronic properties as compared to crystalline silicon. The lack of symmetry and long range order in a-Si:H films makes them not conform to the principle of conservation of momentum [2.1, 2.13], giving them a different optical behaviour compared to c-Si.

The determination of the optical parameters (absorption coefficient, optical band gap and refractive index) of amorphous silicon is usually extracted using computer simulation iterations of electromagnetic transmission or reflection spectra.

These procedures involve using the transmission and the reflection spectra from a UV-Vis spectrophotometer [2.14]. In this work the optical parameters will be determined from the transmission spectra only using the method presented by R Swanepoel [2.15].

On the sample holder of the UV-Vis spectrophotometer, the sample of a-Si:H thin film is placed normal to the UV-Vis radiation. The substrate on which the film was grown has to be transparent to all the wavelengths in the band of interest, and the film is assumed to be uniform and homogeneous.

The optical radiation is then passed through the sample, and this results in a transmission spectrum that also contains an interference pattern due to the thin a-Si:H film only, as shown in figure 2.4. The optical parameters can then be extracted from this transmission spectrum T(λ). The film with thickness d and complex index of refraction n $= n - ik$,

where n is the refractive index and k is the extinction coefficient, has an absorption coefficient that can be expressed as:

$$\alpha = 4\pi \frac{k}{\lambda}.$$ (2.2)

The interference patterns displayed by the a-Si:H film on a glass substrate is due to the a-Si:H thin film only [2.15], the mathematical expression for this transmission is given by equations 2.3.
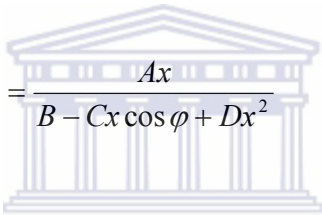
$$T = \frac{Ax}{B - Cx\cos\varphi + Dx^2}$$ (2.3a)

where

$$A = 16n^2 s$$ (2.3b)

$$B = (n+1)^3 (n+s^2)$$ (2.3c)

$$C = 2(n^2 - 1)(n^2 - s^2)$$ (2.3d)

$$D = (n-1)^3 (n-s^2)$$ (2.3e)

$$\varphi = \frac{4\pi n d}{\lambda}$$ (2.3f)

$$x = \exp(-\alpha d).$$ (2.3g)
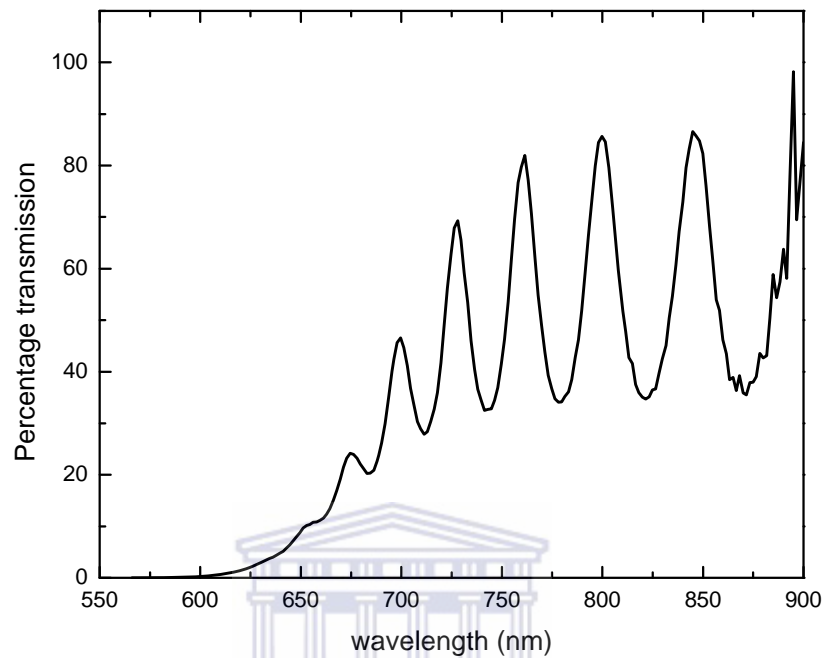
Figure 2.4. A spectrum of a-Si:H film on a glass substrate showing thickness interference fringes.

The two envelopes of the extremes of the interference patterns can be written as

$$T_{Maxima} = \frac{Ax}{B + Cx + Dx^2} \qquad (2.4)$$

and

$$T_{Minima} = \frac{Ax}{B - Cx + Dx^2} . \qquad (2.5)$$

T_{Maxima} and T_{Minima} are considered to be continuous functions of λ and thus of $n(\lambda)$ (refractive index) and $x(\lambda)$ (thickness). This implies that for every T_{Maxima} there is a corresponding T_{Minima} for any λ.

21

2.4.2 Transparent region

The transparent region is the part of the spectrum where it represents transmitted radiation. The transmitted radiation has wavelengths that just pass through the a-Si:H film with negligible absorption. Considering the glass substrate alone the interference free transmission is given by:

$$T_s = \frac{(1-R)^2}{1-R^2} \tag{2.6}$$

where

$$R = \left[\frac{(s-1)}{(s+1)}\right]^2 . \tag{2.7}$$
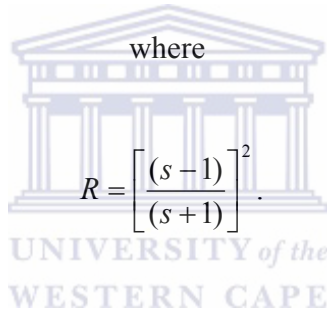
This implies that $x = 1$ (in equation 2.3g) since $\alpha = 0$ for both T_{Maxima} and T_{Minima}. T_{Maxima} can be simplified by substituting in equations (2.3), this will give

$$T_{Maxima} = \frac{2s}{s^2 + 1} . \tag{2.8}$$

The simplified form of T_{Maxima} is the same as the interference free transmission for the substrate T_s. This is because in this region the maxima of interference fringes are a function of s only and coincide with the T_s (substrate transmission). When the wavelength at T_{Maxima} starts to depart from T_s this signifies the beginning of absorption. Simplifying the T_{Minima} expression by substituting in s equations (2.8) yields

$$T_{Minima} = \frac{4n^2 s}{n^4 + n^2(s^2+1) + s^2} \tag{2.9}$$

or

$$n = [N + (N^2 - s^2)^{\frac{1}{2}}]^{\frac{1}{2}} \tag{2.10}$$

where

$$N = \frac{2s}{T_{Minima}} - \frac{s^2+1}{2}. \tag{2.11}$$

T_{Minima} is also a continuous function of both n and s, therefore T_{Minima} can be used to calculate n from equation (2.10).

2.4.3 Region of weak and medium absorption

In these wavelength regions the T_{Maxima} of the film from the transmission spectra begins to diverge from the interference free transmission of the substrate T_s. This denotes the beginning of absorption, hence $\alpha \neq 0$ and $x < 1$.

Subtracting the reciprocal of equation (2.4) from the reciprocal of equation (2.5) yields

$$\frac{1}{T_{Minima}} - \frac{1}{T_{Maxima}} = \frac{2C}{A}. \tag{2.12}$$

23

Substituting equation (2.3) into (2.12) and solving for *n* gives

$$n = [N + (N^2 - s^2)^{\frac{1}{2}}]^{\frac{1}{2}} \tag{2.13}$$

where

$$N = 2s\frac{T_{Maxima} - T_{Minima}}{T_{Maxima}T_{Minima}} + \frac{s^2 + 1}{2}. \tag{2.14}$$

From equations (2.13) $n(\lambda)$ in the region of medium absorption can be calculated using both T_{Minima} and T_{Maxima}.

2.4.4 Region of strong absorption

Over these wavelengths in the transmission spectrum the interference fringes disappear due to strong absorption. This makes it quite impossible to calculate *n* and *x*, these values can only be extrapolated from values in other regions of the spectra.

2.4.5 Determination of the thickness and refractive index

Thickness determination of the film involves the use of the interferometric equation

$$2nd = m\lambda \tag{2.15}$$

where *m* and *n* are the order number and refractive index respectively, *d* is the film thickness and λ is the wavelength. The order number can be determined graphically, by

plotting the half integer for the minima or the integer for the maxima versus $\frac{1}{\lambda}$. The interferometric equation for the extremes of the spectrum takes the form

$$2nd = (m_1 + \frac{k}{2})\lambda \qquad (2.16)$$

where

$$k = 0,1,2,3,4,...$$

This form of interferometric equation alternates between minima and maxima depending on the k value. This is a form of a straight line which has a slope $2d$ and the y-intercept $-m_1$. The straight line is drawn through the first integer for the maxima or through the half integer for the minima. The points that are not lying on the straight line denote the beginning of absorption. By dividing the slope by two, the thickness of the film is obtained.

The values of $n(\lambda)$ can be fitted for each extreme from a function of the form

$$n(\lambda) = \frac{a}{\lambda^3} + n_0, \qquad (2.17)$$

where n_0 is the value of $n_1(\lambda)$ extrapolated to 0 eV and a is constant which is reasonably postulated to be 2.3 [2.15]. The best fit through the points of extrema is taken to obtain a polynomial function for $n(\lambda)$.

2.4.6 Absorption coefficient

The absorption coefficient α is given by

$$\alpha = -\frac{1}{d}\ln|x|.$$
(2.18)

This expression is obtained from

$$x = \exp(-\alpha d)$$
(2.19)

and the extinction coefficient is

$$k(\lambda) = \frac{\alpha\lambda}{4\pi}.$$
(2.20)
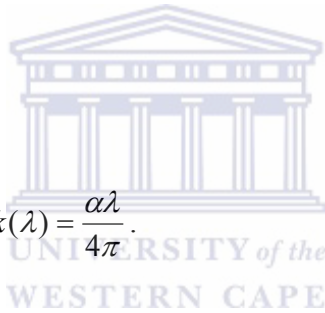
The graph of absorption coefficient is plotted as shown in figure 2.4 to show its relation with the photon energy. Since the absorption coefficient changes with the wavelength, the norm is to compare the absorption coefficient at a specific wavelength like at 600 nm, which is approximately 2 eV. Figure 2.5 displays a plot of the absorption coefficient versus photon energy of a-Si:H thin film.
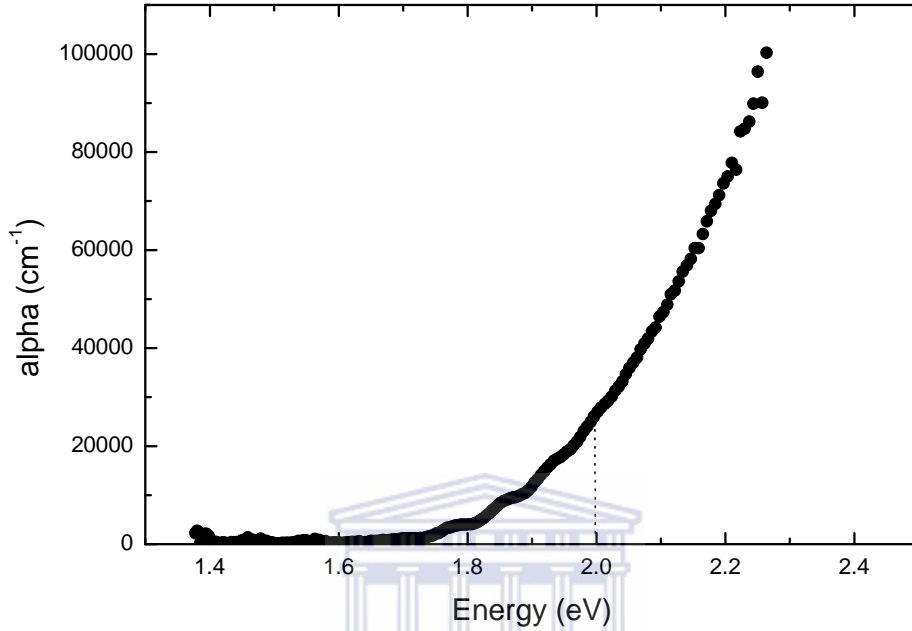
Figure 2.5. The plot of absorption coefficient of a-Si:H thin film in relation to the photon energy.

2.4.7 Theory of optical band gap

An optical band gap is a representation that describes the energy difference between the valence band and the conduction band in a semiconductor. Understanding the role of the density of states and the conductivity of the a-Si:H during the optical processes in the bulk of the material is important. The understanding of these processes will help in determining the optical band gap of a-Si:H. The photoconductivity of amorphous film can be defined as [2.16]

$$\sigma(\omega) = \frac{2\pi e^2 \hbar^3 \Omega}{m^2 \hbar \omega} \int \{f(E) - f(E + \hbar\omega)\} N(E) |P(\omega)|^2 N(E + \hbar\omega) dE . \qquad (2.21)$$

27

This expression describes the transition that takes place in the density of states between the valence band and the conduction band. Here Ω is the volume element containing one electron while $f(E)$ is the Fermi-Dirac distribution. $P(\omega)$ refers to the constant momentum matrix element for the absorption.

The optical absorption is given by the ratio of the photons absorbed per unit area, making the absorption coefficient proportional to the product of the density of the occupied state and the unoccupied states that can be bridged by a photon with energy $h\nu$, provided the transition probability is the same for all states. Using the Fermi-Dirac distribution when T = 0 K, the equation (2.21) can simplified to
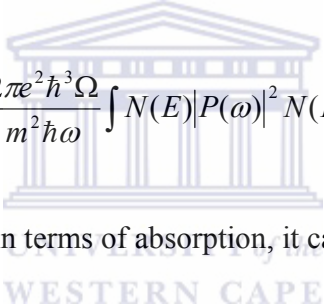
$$\sigma(\omega) = \frac{2\pi e^2 \hbar^3 \Omega}{m^2 \hbar\omega} \int N(E)|P(\omega)|^2 N(E + \hbar\omega)dE. \qquad (2.22)$$

Expressing the equation (2.22) in terms of absorption, it can be rewritten as

$$\alpha(\omega) = \frac{2\pi e^2 \hbar^3 \Omega}{m^2 \hbar\omega\varepsilon_0 n(\omega)c} \int N(E)|P(\omega)|^2 N(E + \hbar\omega)dE. \qquad (2.23)$$

The absorption coefficient is related to the photoconductivity by

$$\alpha(\omega) = \frac{\sigma(\omega)}{\varepsilon_0 n(\omega)c}. \qquad (2.24)$$

If E_a and E_b are the localized states in the mobility edge of the valence and the conduction band respectively, their density of states are given by

$$N_a = N_v \left(\frac{E_a - E}{E_a - E} \right)^p \text{ for E} \leq E_a \qquad (2.25)$$

$$N_b = N_c \left(\frac{E - E_b}{E_c - E_b} \right)^q \text{ for E} \geq E_b. \qquad (2.26)$$

P and q describe the density of states distribution in the valence and conduction bands. By substituting equations (2.24) and (2.26) into (2.23) and integrating over all possible transitions, the solution absorption for the coefficient is given by

$$\alpha(\omega) = \frac{2\pi e^2 \hbar^3 \Omega}{m^2 \hbar \omega \varepsilon_0 n(\omega) c} \frac{\Gamma(p+1)\Gamma(q+1)}{\Gamma(p+q+2)} \times \frac{N_v N_c}{(E_a - E_v)^p (E_c - E_b)^q} \left\langle |P(\omega)|^2 \right\rangle (\hbar\omega - E_g)^{1+p+q}$$

$$(2.27)$$

The momentum transition matrix element for absorption is averaged over all ranges of energy, if it is then assumed to be independent of ω. Equation (2.27) can be simplified to

$$\left[\alpha(\omega) n(\omega) \hbar \omega \right]^{\frac{1}{1+q+p}} = B_g (\hbar\omega - E_g) \qquad (2.28)$$

where B_g is a constant and E_g is the optical band gap [2.16, 2.17].

2.4.8 Calculation of band gap from the T(λ) spectrum

When photons interact with a semiconducting thin film, the photons with the energy greater to the energy band gap are absorbed and those that are less than the energy band gap are transmitted. Tauc [2.17] formulated an expression for determining the band gap for amorphous materials using the optical constant that can be calculated from the transmission spectrum.

$$(n\alpha h v)^{\frac{1}{2}} = \text{constant} \times (h v - E_g) \qquad (2.29)$$

This band gap calculation assumes the density of states near the band edges to be parabolic in nature.

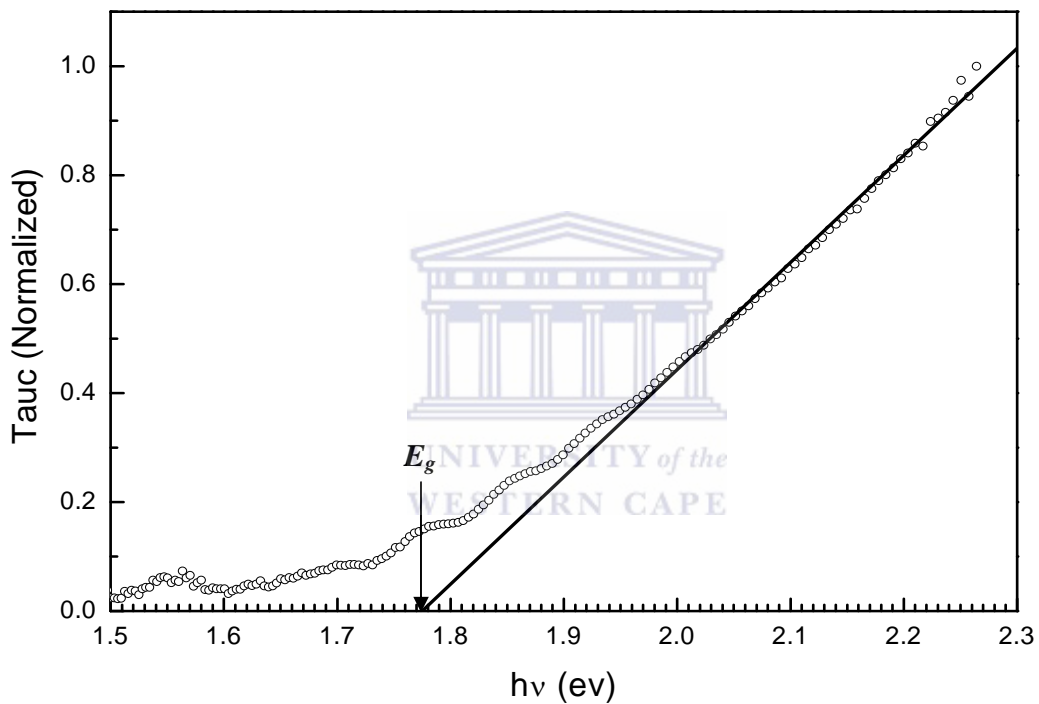**Figure 2.6.** Tauc band gap plots for a hydrogenated amorphous silicon thin film.

The plot of $(n\alpha h v)^{1/2}$ versus $h v$, where $(n\alpha h v)^{1/2}$ (i.e Tauc) is normalized, is shown in figure 2.6 was used to determine the Tauc band gap of a-Si:H thin film. This value was obtained by extrapolating a linear fit of the medium absorption region on the Tauc plot to where it cuts the energy axis.

2.5 Fourier Transform Infrared Spectroscopy (FTIR)

2.5.1 Introduction

Fourier Transform Infrared Spectroscopy (FTIR) is a non destructive analytical technique that uses the photons in the infrared region of the electromagnetic spectrum. These photons have sufficient energy to induce amplified molecular vibrations in the infrared (IR) active side of the sample's molecule. During this process there is a change in the dipole moment of the infrared (IR) active molecule, which results in a signature spectrum of the molecule under investigation when measured [2.18].

2.5.2 Theory

When a beam of electromagnetic radiation is incident on a material, the beam can either be absorbed, transmitted or reflected depending on its frequency and the molecular structure of the material being irradiated. Beams of different frequency can have different effects on the molecules of the substance that is being irradiated. When a beam of electromagnetic radiation which has a frequency in the 1.2×10^{13} Hz to 1.2×10^{14} Hz (infra-red frequency) band is passed through a sample, it effects a transition from one molecular vibrational energy to the next on the IR active molecule [2.19].

The photons of electromagnetic radiation possess energy, hence when a molecule absorbs electromagnetic radiation it gains energy to make a quantum transition from energy level E_1 to E_2. The frequency of the absorbed radiation is associated with the transition energy by Planck's law which is

$$E_1 - E_2 = h v = \frac{hc}{\lambda} \,. \qquad (2.30)$$

31

If there exists an allowed transition that is related to the frequency of the incident radiation by Planck's constant, the radiation will be absorbed, if the transition is forbidden (does not satisfy the Planck's equation) then the incident radiation will be transmitted.

When molecules vibrate, they do so with a frequency characteristic to the molecule, the intensities of these vibrations occur as amplitudes in the FTIR spectrum. Only certain molecular vibrational motions are allowed as permitted by quantum mechanics. In the case of thin films of a-Si:H irradiated by an IR radiation, the IR active hydrogen silicon bonding configurations will absorb IR photon energy. The hydrogen atom that is bonded to silicon in the a-Si:H matrix produces a local vibrating dipole, this is because of the difference in the electronegativity between the hydrogen atom which is negatively charged and the silicon atom which is positively charged [2.19].

In this harmonic oscillator of Si-H, the dynamic dipole moment changes when an IR photon is absorbed by a Si-H oscillator. This result in a vibrational state with a larger vibrational dipole moment, this change in dynamic dipole moment and the concentration of the bonded hydrogen atoms will contribute to the spectral band and its intensity in the IR spectra [2.18]. Figure 2.7 shows the typical setup of the FTIR experiment.
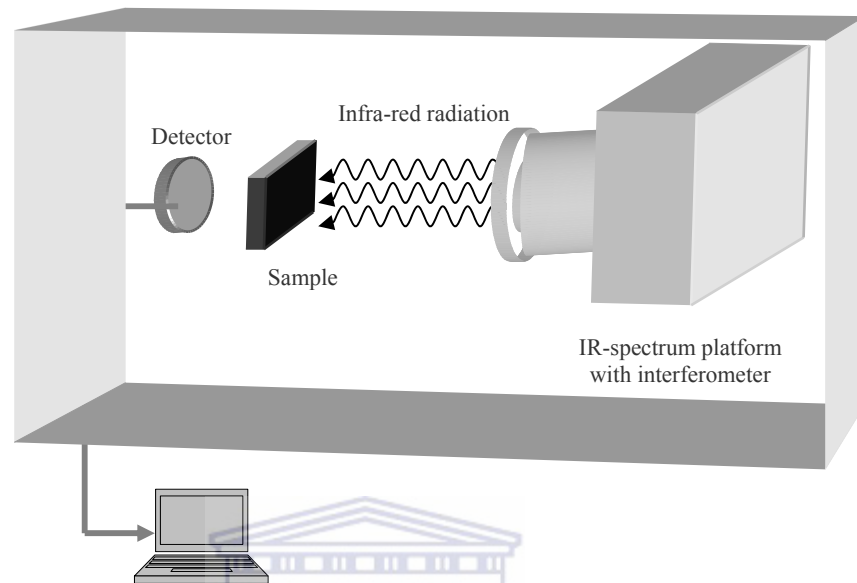
Figure 2.7. Schematic of the FTIR experimental setup.

2.5.3 FTIR in the hydrogenated amorphous silicon technology

The bonding configuration of silicon and hydrogen atoms in a-Si:H film can take several forms. The FTIR spectrometry can give information on the dominant silicon-hydrogen bonding configurations, and also the total concentration of hydrogen bonded to the silicon atoms in a-Si:H film [2.19]. From the FTIR spectroscopy data analysis the structural information of the a-Si:H film can be deduced by calculating the structure factor (R*) of the deposited film, and the percentage of hydrogen in the film can also be calculated [2.6]. The IR active silicon-hydrogen configurations in a-Si:H film are shown in table 2.8.

ENERGY (cm^{-1})	BONDING CONFIGURATION	VIBRATIONAL MODE
630	Si-H, Si-H$_2$, (Si-H$_2$)$_n$, Si-H$_3$	Rocking
845	(Si-H$_2$)$_n$	Bending
880	Si-H$_2$	Bending
890	(Si-H$_2$)$_n$	Bending
2000	Si-H (isolated)	Stretching
2070 – 2100	Si-H (on voids), Si-H$_2$, (Si-H$_2$)$_n$	Stretching
2130	Si-H$_3$	Stretching

Table 2.8. Phonon generation in a-Si:H and their wavenumber [2.6].

2.5.4 FTIR analysis and interpretation

From figure 2.8 it is evident that the 630 cm^{-1} mode is present in all silicon-hydrogen bonding configurations, this mode was found to be independent of preparation method and deposition condition, hence the integrated intensity of this mode is used to calculate the hydrogen concentration in a-Si:H film [2.1, 2.8].

Other vibrational modes shown in figure 2.8 can be interpreted to determine the quality of the grown film. The modes in $800 - 900$ cm^{-1} are associated with film deposited in 'non-optimal' conditions [2.19], this film tends to be void rich and have poor optoelectronic properties. A technological quality a-Si:H film has the Si-H bonding configuration as a predominant one, this stems from the optimum deposition conditions which are usually obtained when the 'optimum' values of the deposition parameters are used [2.20].

The vibrational mode at ~2000 cm^{-1} is due to the change in the dynamic dipole moment when a resonant IR photon is being absorbed by the Si-H molecule in the a-Si:H bulk [2.19, 2.20]. The Si-H configuration might also give a stretch band at ~2100 cm^{-1}. If this band is present without any evidence of spectral modes in the $800 - 900$ cm^{-1} band, then it is proposed that the local bonding structure is a Si-H bond located in a microvoid [2.19].

The mode in the ~2000 cm^{-1} which is from Si-H in the bulk, and that at ~2100 cm^{-1} which is from the Si-H located in a microvoid are used to calculate the microstructure parameter R^*. This is a figure of merit to determine the quality of the grown a-Si:H film. The microstructure parameter R^* is mathematically represented as shown in equation 2.31. The results of this calculation will give an indication of the void structure ratio in the a-Si:H films

$$R^* = \frac{I_{2100}}{I_{2000} + I_{2100}}.$$ (2.31)

For a good quality film the R^* will have a very low value (approaching zero), this signifies a film with a very low concentration of voids in it.

A Brodsky-Cardona-Cuomo (BCC) correction [2.21] procedure was applied in all the FTIR spectroscopy calculations. This was to account for the incoherent reflections and multiple reflections that occur on both the film and the substrate during the FTIR measurement.

2.6 Raman spectroscopy

2.6.1 Introduction

Raman spectroscopy technique is used in this work to study the modes of vibration and rotation of physical systems. This technique is based on the principle of the elastic and inelastic scattering of monochromatic electromagnetic radiation incident to the sample, and this results in the polarization of the molecules in the physical system [2.22].

Raman spectroscopy technique is sensitive to the changes in the small range order in the a-Si:H matrix, from the processed Raman spectrometry data the information on the root mean square bond angle variation can be deduced to quantify the a-Si:H network disorder[2.23].

2.6.2 Theory

When the photons of monochromatic electromagnetic radiation interact with the film of a-Si:H some of the photons are elastically scattered (Rayleigh scattering), while others are inelastically scattered (Raman scattering) by the molecules in the film. As the monochromatic beam passes through the sample, there is a molecular polarizability that is induced on the vibrating atoms in the film due to the intensity of the beam, this is called the Raman effect [2.22]. In the first-order Raman scattering, a photon with frequency ω_o is scattered by the molecules of a-Si:H, this results in a creation or annihilation of a phonon with frequency ω.

When the Raman scattered photon has a new frequency $\omega_o - \omega$ after the scattering event, the scattering process is called the Stokes scattering [2.23]. When an annihilation of a phonon occurs and after the scattering, the photon has a new frequency of $\omega_o + \omega$, the process is called the anti-Stokes scattering. The Stokes first-order scattering intensity $I(\omega)$ for amorphous systems can be expressed using equation 2.32.

$$I(\omega) = C(\omega)g(\omega)\left(\frac{n_{BE}(\omega)+1}{\omega}\right), \qquad (2.32)$$

where the Bose-Einstein (n_{BE}) thermal factor is represented as
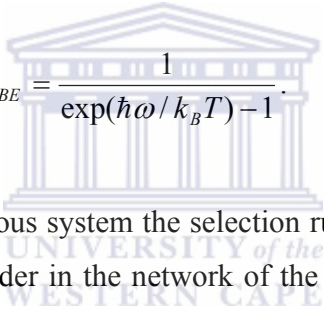
$$n_{BE} = \frac{1}{\exp(\hbar\omega/k_B T)-1}. \qquad (2.33)$$

When dealing with the amorphous system the selection rule for momentum conservation is relaxed, because of the disorder in the network of the amorphous systems. The broad band that is symmetric around 480 cm^{-1} in the Raman spectrum is due to the vibrational density of states, this band mirrors the degree of disorder in the amorphous network of the a-Si:H film [2.23] as shown in figure 2.9. The full width at half maximum (FWHM) of this transverse optical peak (TO) at 480 cm^{-1} (Γ) is related to the root mean square bond angle variation ($\Delta\theta_b$) by the expression

$$\Gamma/2 = 7.5 + \Delta\theta_b \qquad (2.34)$$

The bond angle variation in a-Si:H film ranges between $7.0^{\circ} - 8.2^{\circ}$ and $11.0^{\circ} - 14.1^{\circ}$ [2.23, 2.25], with the lower edge of the limit (7.0°-8.2°) being for films with good short range order, and the upper edge represents films which are maximally disordered.
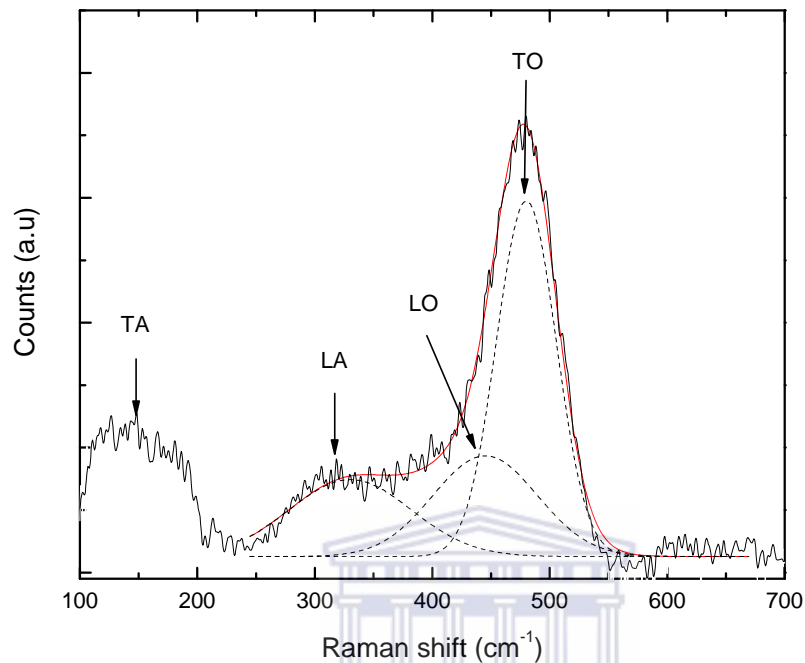
Figure 2.9. Raman spectrum of a-Si:H thin film.

2.7 Rutherford Backscattering Spectrometry (RBS)

2.7.1 Introduction

Rutherford Backscattering Spectrometry is a non destructive technique that is used for the elemental depth profiling of the thin films. It is based on the principle of the collision between the atomic nuclei and a projectile beam of highly energetic, homogeneous and monoenergetic He^{2+} ions that are directed onto a sample mounted in a chamber evacuated to the pressure of 10^{-7} mbar.

This process involves measuring the number and energy of the He^{2+} ions in a beam which backscatters after colliding with the atoms in the sample at which the beam has been targeted. These backscattered ions are measured and counted by a semiconductor nuclear particle detector placed at some angle to the sample in the chamber. The information collected from the backscattered ions by the detector can be used to determine the elemental concentration and their depth below the surface.

2.7.2 Theory

Homogenous and mono-energetic He^{2+} ions are accelerated to an energy of 2 MeV by a Van De Graaff accelerator. These particles are passed through a series of bending magnets and collimators. This beam is then directed onto the sample where the He^{2+} ions of mass m and energy E_o (normally 2 MeV) collide with the target atoms of mass M. This collision between the beam and the sample's atoms does not involve direct contact between the He^{2+} and the nuclei of the sample's atoms. There is an exchange of energy between the nuclei of the He^{2+} and the sample's atomic nuclei due to the coulombic interaction. This interaction can be represented accurately using classical mechanics.
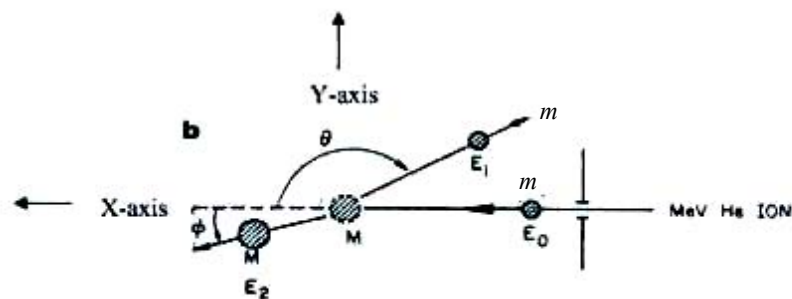

Figure 2.10. Schematic of the RBS experimental set up [2.27]

The conservation of momentum and energy in the X and the Y axis are given by the following equations 2.35, where M is the atomic nucleus and m is the mass of the alpha particle (He^{2+}) as shown in figure 2.10:

Energy   : $$\frac{1}{2}Mv^2 = \frac{1}{2}Mv_1^2 + \frac{1}{2}mv_2^2$$ (2.35)

Momentum in the X-axis: $Mv = Mv_1\cos\theta + mv_2\cos\varphi$ (2.35a)

Momentum in the Y-axis: $0 = Mv_1\sin\theta - mv_2\sin\phi$.   (2.35b)

As the He^{2+} beam passes through the sample it loses energy mainly due to two processes (electronic stopping power and the elastic scattering process). Firstly the energy lost is dependent on the beam's particle mass and the mass of the target atoms, because the He^{2+} nucleus and the sample nucleus experience elastic scattering and lose some energy during the process. On the other hand the electronic stopping power of the material contributes to the energy loss as the He^{2+} beam traverses the material. The final energy of the backscattered beam that will be collected by the detector will be less than that of the incident beam energy. The ratio of the beam before and after the collision is called the *kinematic factor* which is beam particle mass and target atoms dependent. Assuming the conservation of momentum and kinetic energy, the kinematic factor can be presented as follows,
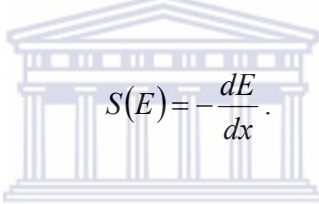
$$K = \frac{E_1}{E_0} = \left[\frac{\left(M^2 - m^2\sin^2\theta\right)^{1/2} + m\cos\theta}{M + m}\right]^2 .$$ (2.36)

The backscattering of the He^{2+} takes place with a known cross section given by

$$\frac{d\omega}{d\Omega} = \left[\frac{zZe^2}{4E}\right]^2 \times \left(\frac{4}{\sin^4\theta}\right) \times \frac{\left[\left(1-\left(\frac{m}{M}\times\sin\theta\right)^2 + \cos\theta\right)\right]}{\left[1-\left(\frac{m}{M}\times\sin\theta\right)^2\right]^{\frac{1}{2}}}, \quad (2.37)$$

where z and Z are atomic numbers of the beam particle and the target atoms respectively; ω is the detector solid angle.

The energy lost by the He^{2+} particles due to electronic interaction as they penetrate deep into the sample is given by

$$S(E) = -\frac{dE}{dx}. \quad (2.38)$$

This is called the stopping power of the material and is dependent on the electron distribution of the target atoms, and varies with respect to the distance traversed in the material [2.26, 2.27].

The backscattered He^{+2} particles that are collected by the nuclear solid state detector are energy sorted by the system's electronics, from these a RBS spectrum is displayed showing the number of the backscattered He^{2+} versus the energy (channel) of the spectrum.

The Van De Graaff accelerator real time RBS spectrometry at iThemba LABS Faure MRD division was used to analyze the *Aluminium Induced Crystallization P-Doped* (**AICPD**) thin film grown on aa Corning glass substrate. The sample was mounted on the heater in the RBS chamber, and the sample was heated from room temperature to 375 ^{o}C at the ramping rate of 3 ^{o}C/min and a set pressure of 1×10^{-7} mbar.

All the RBS analyses were done using the Rutherford Universal Manipulator Program (RUMP) for quantitative analysis.

2.8 Energy Dispersive X-ray Spectroscopy (EDS)

2.8.1 Introduction

The p-doped film that was grown using the *Aluminium Induced Crystallization P-Doped* (*AICPD*) process was quantitatively analyzed using the scanning electron microscope in the EDS mode. The percentage of the aluminium that was incorporated in the a-Si:H film by bonding with silicon atom during the deposition process, was determined from the HITACHI X-650 Scanning Electron Microanalyzer in the EDS mode with a sensitivity of 139 eV.

2.7.2 Energy Dispersive Spectroscopy (EDS) theory

The electrons used in the energy dispersive spectroscopy are produced by a hair-pin shaped tungsten filament. The filament was heated up to overcome the work function of the metal. This tungsten hair-pin is cased in the Wehnelt cylinder which makes up part of the electron gun. The electron gun is connected to the negative pole of a high voltage supply and is located at the top of the microscope. The filament is negatively charged to a high electrical potential which causes the electrons to be accelerated towards the anode. This potential difference is in the order of several keV's.

The accelerated electrons pass through the aperture in the anode which trims off peripheral electrons and allows the rest through. The electrons that pass through the anode aperture diverge below this point and the electromagnetic lenses are used to converge these spread out electrons.

The first set of these lenses is the condenser lens and this lens causes the electrons to converge and pass through a focal point, which is generally above the condenser aperture. The electron beam that passes through the condenser aperture is now more condensed and homogeneous with the scattered and inhomogeneous parts being trimmed off [2.28].

The electron beam will continue down the column and again diverge below the condenser lens aperture, here a final electromagnetic lens is used to focus the electron beam at the specimen by demagnifying it to the focal point on the specimen.

When a beam of electrons interacts with a specimen, one of the important processes that take place is the emission of characteristic x-rays from the constituent atoms of the specimen. The energy levels between the shells of one atom differ from the other atoms. This characteristic makes the energy necessary to knock an electron off its shell unique to that element. An energetic photon (x-ray) is released when an electron from a higher energy level fills the vacancy of the knocked off electron and during this process an x-ray that has a unique energy to that element is emitted. The energy of this x-ray can then be used as a qualitative way of analyzing the specimen [2.28].

2.8.3 EDS application in doped a-Si:H

Hydrogenated amorphous silicon (a-Si:H) can be doped either n-type or p-type. To determine the amount of dopant that is incorporated in the a-Si:H matrix the EDS technique is used. The fact that every element has a unique characteristic x-ray as explained in the theory is used to determine the amount of dopants in the a-Si:H film. The atomic percentage of the aluminium in the p-doped a-Si:H was determined using EDS spectrometry.

2.9 HALL EFFECT TECHNIQUE

2.9.1 Introduction

When a conducting material has an electric current flowing perpendicular to an external applied magnetic field, a voltage gradient is developed which is perpendicular to both the applied magnetic field and the electric current. This phenomenon is called the Hall Effect (E.H. Hall) [2.29], which is a useful technique in determining electrical conducting properties of semiconductors. The thin films of p-doped films and n-type a-Si:H were probed using the LakeShore 7600 Hall Effect machine at the University of Cape Town for an electrical properties study.

2.9.2 Theory

Electric current in a semiconducting material consists of charged carriers, usually electrons and holes; when these moving charged particles experience a force due to a magnetic field applied perpendicular to their motion they experience a Lorentz force:

$$F_L = -qvB . \qquad (2.39)$$

This forces the charge carriers to move towards the sides of the film, as a result the charges are accumulated on the side of the material. During this process there is an equal but oppositely charged carriers that are left on the other side of the material. An electric field is created between the two sides of the sample due to the separation of charges. The electric field produces a force $F = qE$ which cancels the Lorentz force (this happens instantaneously), once the equilibrium between the two forces have been reached

a potential drop is established across the sides of the sample. This transverse voltage is called the Hall voltage V_H [2.30] and its magnitude is given by equation 2.40

$$V_H = \frac{IB}{qnd} .$$ (2.40)

Figure 2.11 shows the schematic of the Hall Effect theoretical model.
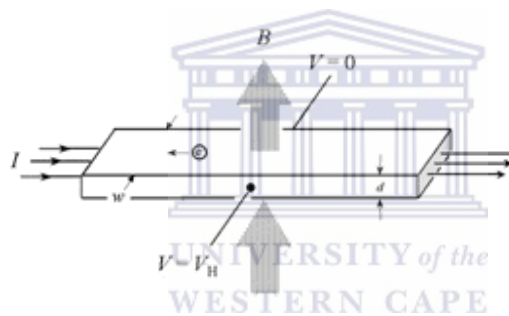

Figure 2.11. The schematic representation of the Hall Effect theoretical model [2.30].

From the Hall voltage the sheet *carrier density* (the amount of carriers in the monolayer) of the conducting material can be found from the expression

$$n_s = \frac{IB}{q|V_H|} .$$ (2.41)

where

I = current

B = applied magnetic field

q = elementary charge

V_H = Hall voltage.

The bulk carrier density of the material can be obtained once the thickness of the material is known and substituted in this expression ($n_s = nd$).The other useful quantities that can be calculated from the Hall Effect is the sheet resistance and the Hall mobility, these can be calculated from the equation below.

$$\mu_{sheet} = \frac{|V_H|}{R_s IB} = \frac{1}{qn_s R_s} \qquad (2.42)$$

The bulk resistivity is determined from $\rho = R_s d$.

2.10 Dark and Photo-Conductivity

The dark conductivity σ_d of a-Si:H thin films can be determined by depositing a thin film on a highly resistive glass. Two coplanar strips of metal preferably with a length that is much greater than the space between the strips should be deposited on the film. This is done to minimize the fringe effect at the ends of the coplanar strips.
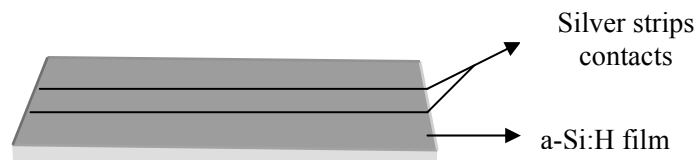

Figure 2.12. A basic geometric schematic of dark conductivity measurement set up.

One centimeter long coplanar strips are deposited on the a-Si:H film to give ohmic contact for analysis. The metal should be such that it has a low work function [2.1]. The coplanar strips are deposited less than 1 mm apart and the film that is to be analyzed should have a thickness in the order of one micron, to prevent the charge depletion extending in a region larger than the exposed region [2.1]. This is because the separation between the strips should be much more than the thickness of the film, with a ~1μm film and a 1mm strip separation this requirement is satisfied.

A compartment box to prevent any stray light was used to house the sample for analysis. A voltage of 100 V was applied across the coplanar contacts and the current passing through the film was measured by a sensitive multimeter in the current mode. Dark conductivity was then calculated from the expression
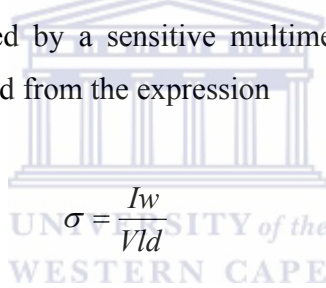
$$\sigma = \frac{Iw}{Vld}$$

where

I = current

V = applied voltage

d = thickness of a-Si:H film

w = distance between the contacts

l = length of the contacts.

The dark conductivity was measured in the dark by putting the sample in a compartment box. On the other hand the photoconductivity can be measured using the same sample geometry. The sample is illuminated with 100 mW/cm^2 of light from the solar simulator and the current measured flowing between the contacts is due to the photo generated carriers in the film.

References:

[2.1] R.E.I. Schropp and M. Zeman, *Amorphous and microcrystalline silicon solar cell: Modeling, Materials and Device Technology*, Kluwer Academic Publisher (1998).

[2.2] E.C. Molenbroek*, Deposition of hydrogenated amorphous silicon with the hot – wire technique* (P.hD. Thesis, University of Colorado, 1995)

[2.3] K. Tonokura, K. Inoue, M. Koshi. *J. Non-Crystalline Solids*, **299-302** 25-29 (2002)

[2.4] M. Konagai, T. Tsushima, M.K. Kim, K. Asakusa, A. Yamada, Y. Kudriavtsev, A. Villegas, R. Asomoza, *Thin Solid Films* **395**, 152-156 (2001).

[2.5] P.A.T.T. van Veenendaal. Ph.D thesis, Utrecht University , 1998

[2.6] R .A. Street*, Hydrogenated amorphous silicon, Cambridge University Press* (1991).

[2.7] S.R. Jadkar, J.V. Sali, S.T. Kshirsagar, M.G. Takwale, *Solar Energy Materials & Solar cell* **85** 301 – 312 (2005).

[2.8] S.R. Jadkar, V. Jaydeep, D.V. Musale, S.T. Kshirsagar, M.G. Takwale*, Solar Energy Material & Solar Cells* **71** 153 – 167 (2002).

[2.9] S.R. Jadkar, J.V. Sali, S.T. Kshrisagar, M.G. Takwale. *Thin Solis Films.* **437** 18 – 24 (2003).

[2.10] N. Honda, A. Masuda, H. Matsumura, *J. Non-Cryst. Sol*. **266-269** 100 (2000)

[2.11] R. Bucher, MatSci XRD Course reader manual, 2004

[2.12] B.D. Cullity. Elements of X-ray diffraction, Addison- Wisley Publishing Company, Reading, Massachusetts (1978)

[2.13] K.F. Feenstra, *Hot-wire chemical vapour deposition of amorphous silicon and the application in solar cells*, Ph.D thesis, Utrecht University , 1998.

[2.14] J.C. Manigacier, G.J. Gasiot, J.P. Fillard, *Journal of Physics. E: Scientific Instruments*. **9** 1002 – 1004

[2.15] R. Swanwpoel, *Journal of Physics. E: Scientific Instruments*, **16** 1214 – 1222. (1983)

[2.16] N.F. Mott, E.A. Davis Electronic Processes in Non-crystalline materials, Clarendon Press, Oxford, U.K. (1971)

[2.17] J. Tauc, Optical Properties of Solids, edited by F. Abeles (North-Holland, Amsterdam, the Netherlands) **277** (1972).

References:

[2.18] Lau, W.S. Infrared characterization for microelectronics. World Scientific. ISBN 9810223528 (1999).

[2.19] Properties of Amorphous Silicon and it's Alloys. Edited by Tim Searle. An INSPEC Publication, emis Data Review series. **19.** ISBN 0852969228

[2.20] R. Ruther, J. Livingstone, *Infrared Physics & Technology* **37** 533 – 537 (1996).

[2.21] M.H. Brodsky, M. Cardona, J.J. Cuomo, *Physics. Review*: **B16** 3556 (1977)

[2.22] H.H. Willards, L.L. merritt Jr. J.A. Dean and F.A. Settle Jr. Instrumental Methods of Analysis 7th Edition, Wadsworth Publication. Co. (1988)

[2.23] D. Beeman, R. Tsu, M.F. Thorpe, *Physical Review*. **B32** 874 (1985)

[2.24] F.L. Galeener, P.N. Sen, *Physical Review*. **B17** 1928 (1978)

[2.25] A.J.M. Bernsten, Ph.D thesis, University of Utrecht, The Netherlands (1993)

[2.26] MatSci Advanced Analytical Method Course Reader (2004)

[2.27] L.C. Feldman, J.W. Mayer, Fundamentals of Surface and Thin Film Analysis, North-Holland Publishers, Amsterdam (1996)

[2.28] M.T. Postek, Jr., Ladd Research Industries, Inc, SCANNING ELECTRON MICROSCOPY. A STUDENT'S HANDBOOK

[2.29] P.M. Fishbane, S. Gasiorowicz, S.T. Thornton, Physics for Scientist and Engineers Prentice Hall International, Inc 2nd Edition (1996)

[2.30] http://www.eeel.nist.gov/812/

Chapter 3

RESULTS AND DISCUSSION

3.1 INTRINSIC LAYER

3.1.1 Introduction

The first solar cell devices using the a-Si:H film technology had a Schottky barrier configuration [3.1], due to the lifetime of the photo-excited free charge carriers being too short. This is because of the higher density of defects introduced by dopants in the doped a-Si:H. The Schottky barrier configuration was replaced by the n-i-p and the p-i-n cell configurations. Figure 3.1 shows a schematic representation of the n-i-p and the p-i-n solar cell configurations.

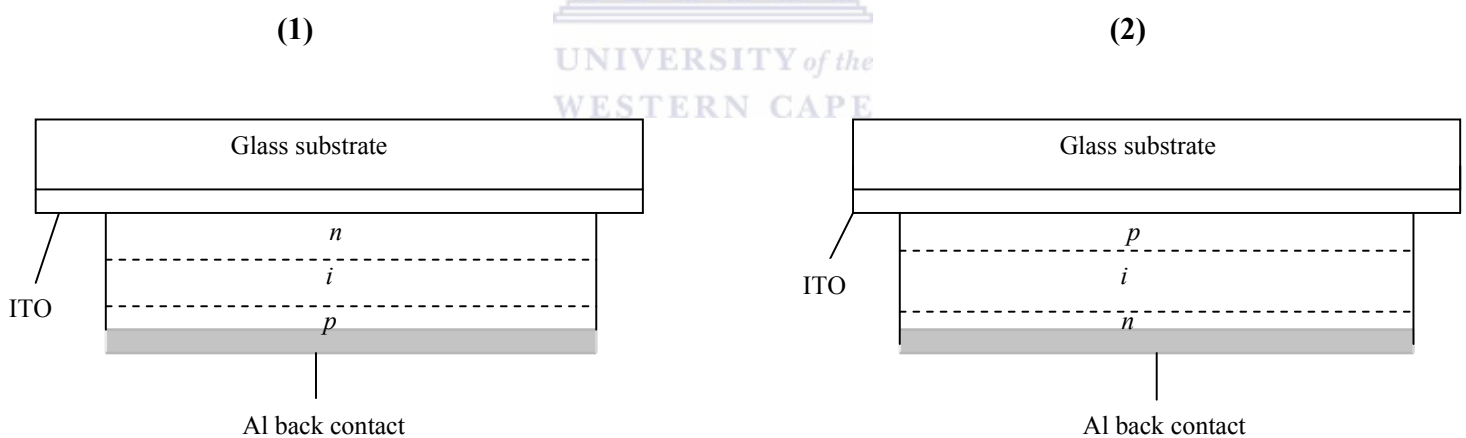**Figure 3.1.** Schematic diagram of a *n-i-p* **(1)** and *p-i-n* **(2)** solar cell configuration on a glass Indium Tin Oxide (ITO) substrate.

In the n-i-p or p-i-n structure, the intrinsic (i) film acts as an active layer, this is because the longer lifetime of the photo-excited charged carriers. [3.2]. That makes it possible for the carriers to be spatially separated and exhibit photovoltaic activity [3.2].

The long lifetime of the photo-excited charged carriers in the intrinsic layer is due to the lower density of defects in this layer.

The intrinsic layer is grown such that it has optical properties (band gap and absorption coefficient) to absorb most photon energy above a certain energy incident from the sun. These photons then excite electrons from the valence band to the conduction band and in the process create holes in the valence band. The electric field created between the n- and the p-layer sandwiching the intrinsic layer, drift the spatially separated electrons and holes to the doped layers [3.2]. These drifted charge carriers in the intrinsic film generate the electric current.

In the n-i-p and p-i-n device structures the intrinsic layer has the largest effect on the performance of cell [3.3], this leads to a need to grow a good quality intrinsic layer for application in a solar cell.
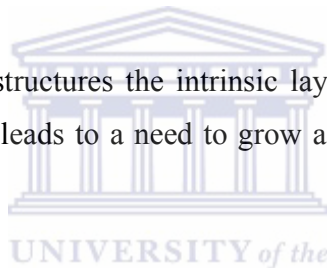
3.2 DEVICE QUALITY a-SI:H FILM

3.2.1 Deposition conditions

The intrinsic a-Si:H films can be grown at various values of deposition parameters in the HWCVD chamber. Each parameter has an effect on the quality of the resulting film during the deposition as explained in chapter two.

A range of values for the deposition parameters were used to grow a-Si:H films on Corning 7059 and polished single crystalline substrates for analysis. The deposited films were grown such that the thicknesses of the films were approximately the same (i.e. ~1 μm, a value recommended for a-Si:H analysis [3.4]). Table 3.1 gives a set of deposition parameters used to grow a-Si:H films. Optimum values for the growth of the films

were selected from a range for which the desired films properties were expected, these ranges or values were based on previous experimental work done in the group.

Table 3.1. Deposition parameters and their values for the a-Si:H films.

Deposition parameters	set values
Filament temperature	1800 ^{o}C
Substrate temperature	200 ^{o}C and 280 ^{o}C
SiH$_4$ flow rate	50 sccm
Pressure	40 μbar, 60 μbar and 80 μbar
Substrate to filament distance	1.8 cm

The growth process of the deposited a-Si:H films from the pyro-catalytic interaction of silane (SiH$_4$) gas with the heated tantalum wire (*primary reaction*), to the nature of the *secondary reaction* of silicon and hydrogen atoms on their way to the heated substrate, to the reaction of the silicon hydrides on the substrate are influenced by the chosen values of the deposition parameters. The resulting atomic structure and the quality of the grown films on a substrate is a result of the chosen values of all the deposition parameters.

3.2.2 XRD spectroscopy

The deposited a-Si:H films on Corning glass were characterized for atomic structure using a θ - 2θ D8 Advanced Bruker XRD spectroscopy machine at iThemba LABS, Faure.

Choosing the optimum deposition conditions is important when it comes to growing films of a-Si:H for device application. This is because in some deposition regimes the resulting film may have atomic arrangements other than the desired amorphous structure.

All the XRD spectra of the samples were substrate corrected to eliminate the contribution of the glass substrate. The XRD spectrum of the substrate is as shown in figure 3.2 below.
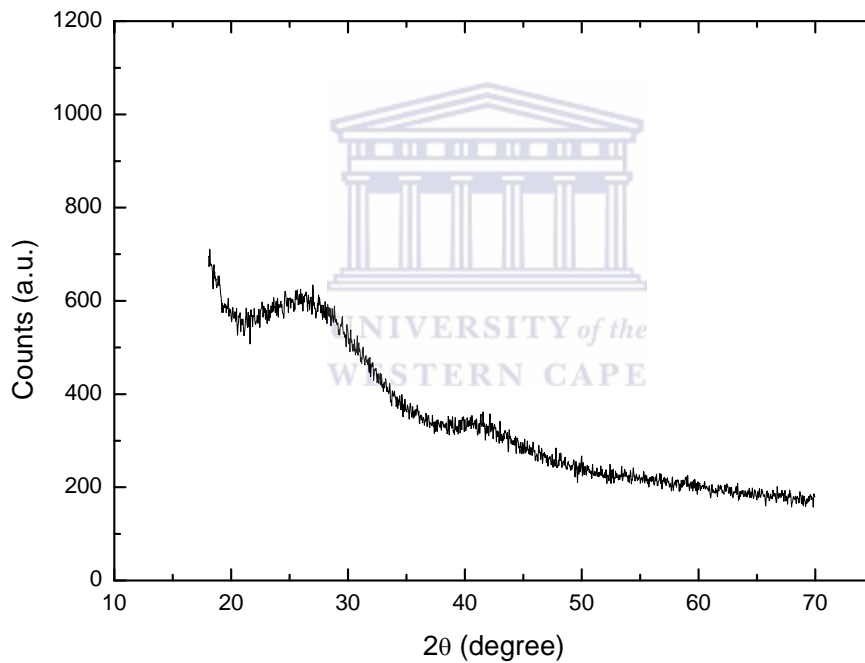

Figure 3.2. The XRD spectrum of the glass substrate.

This spectrum was subtracted from the XRD spectrum of the a-Si:H film on the glass substrate, which has a contribution from both the glass substrate and the film. The XRD spectrum of a-Si:H film on glass is as shown in figure 3.3.
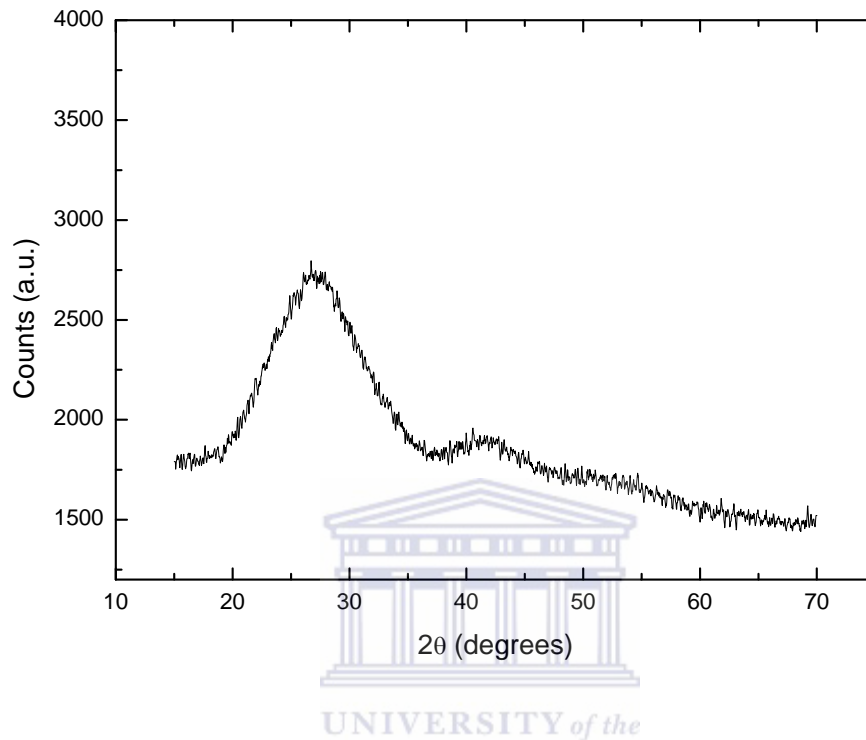
Figure 3.3. The XRD spectrum that shows the contribution of both the a-Si:H film and glass substrate.

The resulting spectrum from the subtraction of the XRD spectrum of the a-Si:H film on glass substrate from the XRD spectrum of the glass gives the XRD spectrum without the contribution of glass substrate. All the plots in figure 3.4 are the XRD spectra of a-Si:H film contribution only. The XRD spectroscopy performed on the deposited films under various deposition conditions showed a broad hump around the 28 $^{\circ}$ on the 2θ scale as shown in figure 3.4.

Figure 3.4. XRD spectra of a-Si:H films grown at varying values of the deposition parameters.

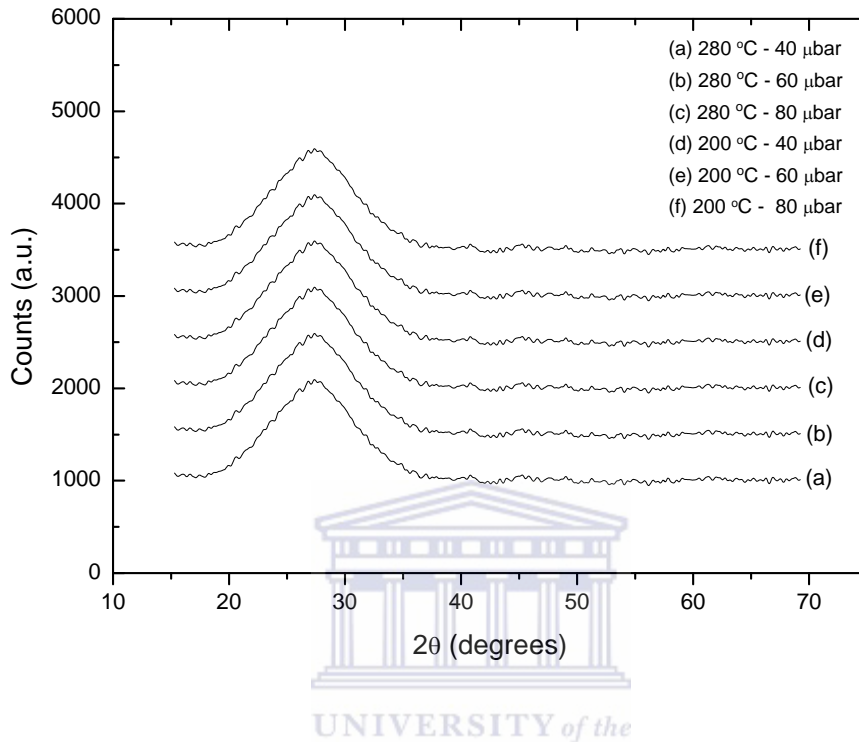A Gaussian distribution was fitted at 28° on the XRD spectra of all the films to compare the medium range order of the films. XRD features at smaller angles involve the correlation of the medium range order [3.5-3.8]. The FWHM of the amorphous hump that appears at small angles has been linked with the medium range order in the film [3.7]. The medium range order variation of the films deposited at the substrate temperatures of 200 $^{\circ}$C and 280 $^{\circ}$C, and various values of the operational pressures evolves as will be shown from the FWHM of the Gaussian fitted at 28° of the spectra in figure 3.4 above.

From the plot in figure 3.5 it is observed that the FWHM of the Gaussian fitted at 28 $^{\circ}$ gets narrower as the deposition pressure increases. This observation suggests that the medium range order of the films improves as the deposition pressure increases.
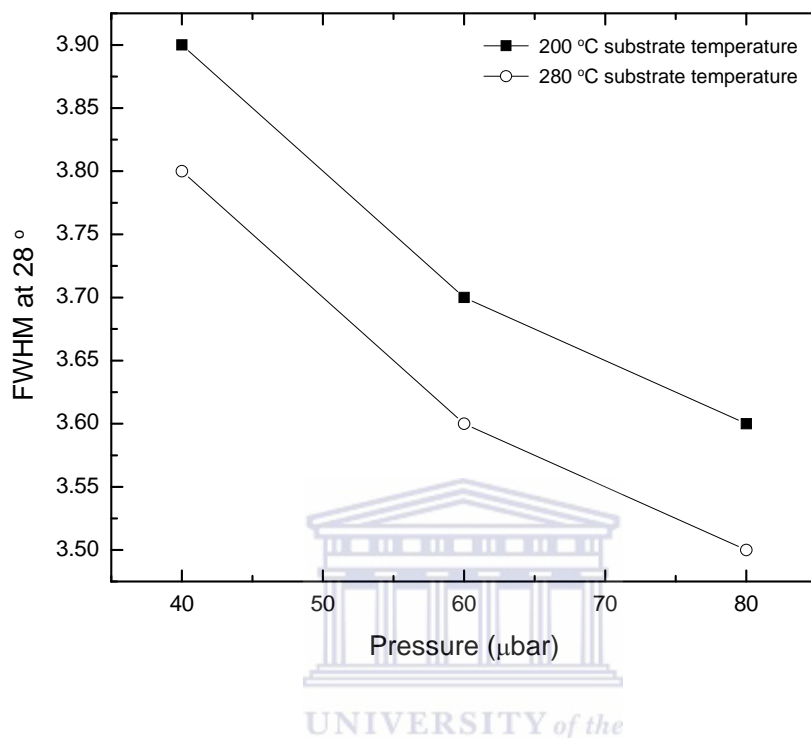
Figure 3.5. Plot of a-Si:H films FWHM fitted at 28 $^{\circ}$ versus deposition pressures at the substrate temperatures of 200 $^{\circ}$C and 280 $^{\circ}$C.

This can be interpreted as the improvement in the medium range order, which is the structural ordering on a length larger than the nearest neighbour in the amorphous matrix [3.5-3.8]. The decrease in the value of the FWHM of a Gaussian fitted at 28 $^{\circ}$, can also be interpreted as a relaxation in the amorphous silicon network taking the structure closer to that of tetrahedral silicon [3.9].

Films deposited at the same operational pressures but having different substrate temperature exhibit a trend, which shows that at higher substrate temperatures (280 $^{\circ}$C) the FWHM of the Gaussian fitted around 28° also decreases. This shows that the substrate temperature has an influence on the structure of the grown film. From these observations

56

it can be said that the operational pressure and the substrate temperature values have a direct effect on the resulting structure of the grown film.

This medium range ordering is proposed to be due to the nature of the *secondary reactions* (silicon and hydrogen atoms from fragmented silane) of the silicon and hydrogen atoms on their way to the heated substrate, and also the reaction of the silicon hydrides when they agglomerate and coalesce on the heated substrate at the processing pressure and substrate temperature.

We presume that as the operational pressure and the substrate temperature values are increased towards their 'optimum regimes', there are enough SiH_3 radicals in the reaction chamber when operating at the optimum pressure. The SiH_3 radicals due to their stability migrate long enough on the heated substrate till they find suitable reactive dangling bonds resulting in a better quality a-Si:H as proposed by [3.10-3.11] and [3.2].

The perfect tetrahedral structure in a-Si:H films is difficult to achieve because of the inherent defects such as the distorted bond angles and bond lengths in a-Si:H films [3.1].

3.2.3 Raman spectroscopy

The short range order of the deposited films was determined from the Raman spectroscopy technique, this technique was chosen because of its sensitivity to small changes in the bond angle variation in the amorphous matrix [3.12]. This was also performed to verify that the films deposited were purely amorphous in nature and had no inclusion of small crystals in the amorphous matrix. The Raman characterization was performed at the CSIR Pretoria.

The Raman spectroscopy data was de-convoluted as shown in figure 3.6 to extract the modes of interest and quantify their contribution in the a-Si:H film.
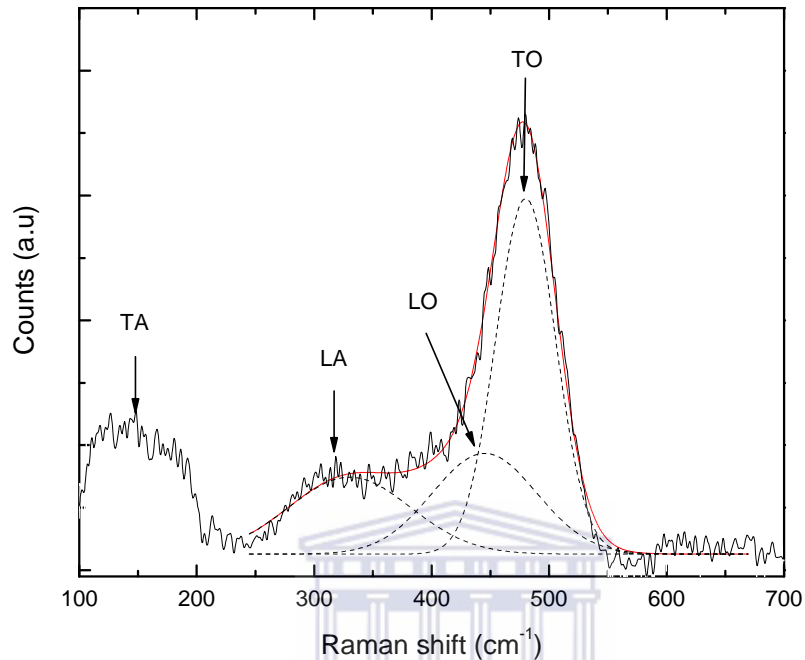
Figure 3.6. The de-convoluted Raman shift spectroscopy spectrum showing the contribution of the modes of interest.

The Raman shift spectra of the films deposited at the substrate temperature of 200 $^{\circ}$C and varying operational pressures are plotted in figure 3.7. The Raman spectra in figure 3.7 were fitted with 3 Gaussians peaks at 480 cm^{-1}, 445 cm^{-1} and at 330 cm^{-1}. The peaks of these fits are due to the phonon modes of transverse optic (*TO*), longitudinal optic (*LO*) and longitudinal acoustic (*LA*) modes. These peaks correspond to the complete amorphous contribution in the a-Si:H film. For a film with crystallites inclusion in the amorphous matrix there is usually a broad shoulder or a peak at the 520 cm^{-1}and this mode is due to the crystalline silicon. From the spectra in figure 3.7 there is no evidence of the 520 cm^{-1} mode appearing.

Figure 3.7. Raman shift spectra of a-Si:H films deposited at the substrate temperature of 200 ^{o}C and their preset operational pressures. The dash line at the 520 cm^{-1} shows the absence of this mode.

The Raman spectroscopy results serve as a complementary technique to substantiate the fact that the grown films are purely amorphous, as previously presented from the XRD spectroscopy.

The films that were deposited at the substrate temperature of 280 ^{o}C were also characterized by Raman spectroscopy. The Raman shift spectra of the films are as shown in figure 3.8. The absence of the 520 cm^{-1} in these spectra also serves as evidence that there are no crystallites inclusions in the film, and the films are purely amorphous as also shown from the XRD spectra of the films.
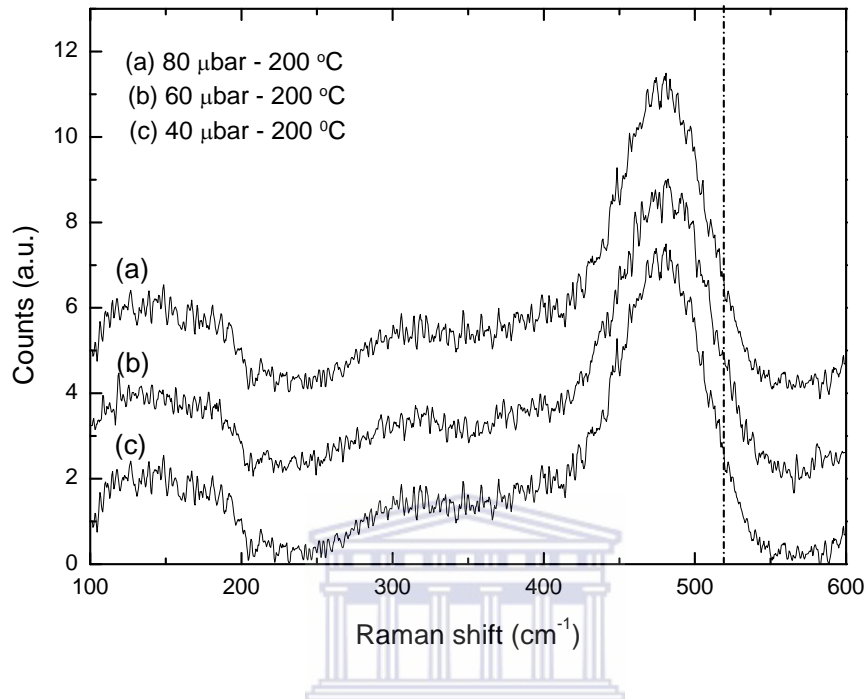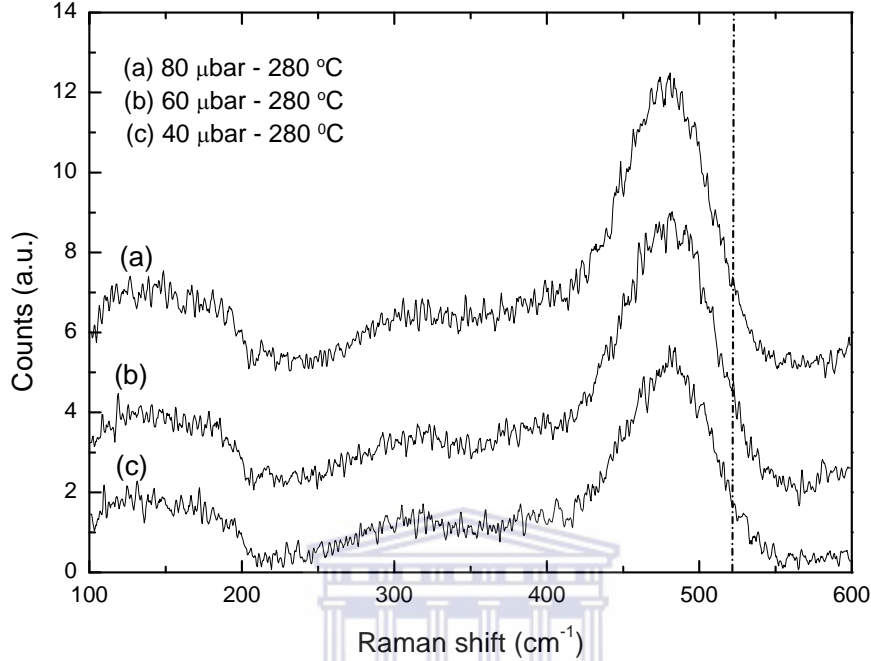
Figure 3.8 Raman shift spectra of the a-Si:H deposited at 280 ^{o}C substrate temperature and their preset operational pressure. The dash line at the 520 cm^{-1} shows the absence of this mode.

The *TO* mode (480 cm^{-1}) from the Raman spectra is normally used to determine the bond angle variation $\Delta\theta$ in the a-Si:H films. The bond angle $\Delta\theta$ variation in a-Si:H film ranges between $7.0^{o} - 8.2^{o}$ and $11.0^{o} - 14.1^{o}$ [3.13], with the lower edge of the limit (7.0^{o}-8.2^{o}) being for films with good short range order and the upper edge represent films which are maximally disordered. The degree of the bond angle variation in a-Si:H film can be deduced by a model proposed by Beeman [3.14]. The root-mean-square bond angle variation ($\Delta\theta_b$) can be related to the Raman spectrum *TO* mode (Γ) full width of half maximum (FWHM) by:

$$\frac{\Gamma}{2} = 7.5 + 3\Delta\varphi_b . \tag{3.1}$$

60

This relationship is linear and the $\Delta\theta_b$ increases with broadening of the *TO* mode. The plot of the $\Delta\theta_b$ at different values of substrate temperatures, against the operational pressures of the deposited films shows the variations in the degree of the $\Delta\theta_b$ of the films as the pressure increases.
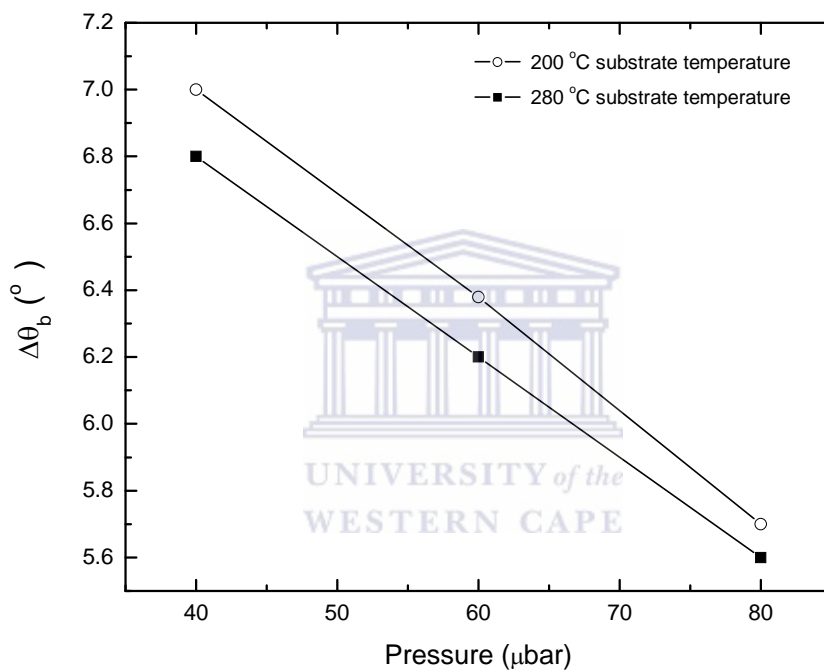
Figure 3.9 A plot of bond angle disorder of a-Si:H versus the operational pressure at different values of substrate temperatures.

The plots in figure 3.9 show a trend similar to that observed when the FWHM of the Gaussian fit at 28 ^{o} from the XRD spectra were plotted, but here the improving ordering from figure 3.9 is that of the bond angles. The plots in figure 3.9 serve as complementary techniques to confirm the improved ordering in the matrix of a-Si:H at elevated operational pressures and substrate temperatures.

This analysis leads us to believe that at these deposition conditions (elevated pressure and substrate temperature) the grown films lean more towards a structure similar to that of a tetrahedral. This is because the medium range order from the XRD spectroscopy improves for films grown at these conditions, and the short range order from the Raman spectroscopy analysis shows an improvement of the short range order due to minimal angular distortion.

3.3 FOURIER TRANSFORM INFRARED (FTIR) SPECTROSCOPY

3.3.1 Hydrogen concentration and Microstructure

The silicon-hydrogen bonding configuration and the hydrogen concentration in the a-Si:H films has a direct influence on the optoelectrical properties of the film [3.1,3.12]. The hydrogen concentration and its bonding configuration to the silicon atoms plays a huge part in the band gap value, the strain in the a-Si:H network [3.15] and on the microstructure factor (R*) of the grown films [3.1]. These are dependant on the deposition parameters used to grow the films. The FTIR spectroscopy was used to determine the dominant silicon-hydrogen configurations, the calculation of the hydrogen concentration and the microstructure factor R* of the films.

The FTIR spectra in figures 3.10 and 3.11 are for films deposited at the substrate temperature of 200 ^{o}C and 280 ^{o}C respectively, and various values of the deposition pressures. The 640 cm^{-1} mode integrated absorption from the FTIR spectra, was used to calculate the hydrogen concentration in the deposited films. This mode was chosen because it includes all the silicon-hydrogen configuration vibrational modes of a-Si:H. The Brodsky-Cardona-Cuomo (BCC) correction was used when doing all the calculations, this was to take into account the effect of incoherent reflections.

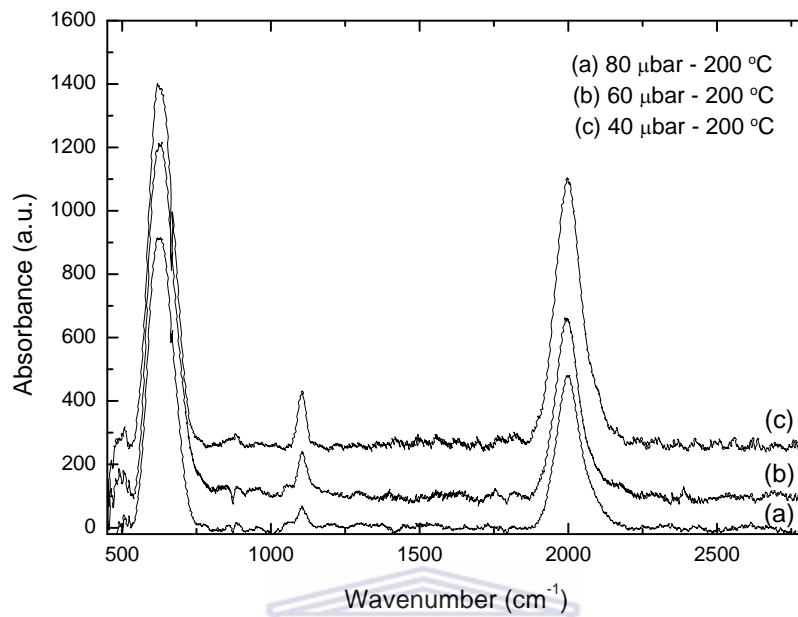**Figure 3.10** BCC corrected FTIR spectra of a-Si:H films deposited at 200 °C substrate temperature and varying pressures.
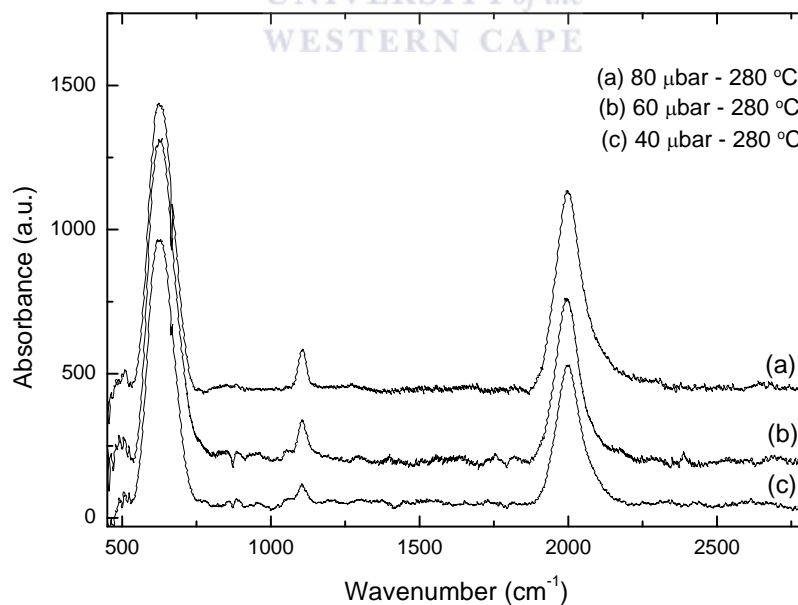
Figure 3.11 BCC corrected FTIR spectra of a-Si:H films deposited at 280 °C substrate temperature and varying pressures.

The hydrogen concentration in the grown film has an important effect on the optoelectrical properties of the a-Si:H film. Varying concentrations of hydrogen are incorporated in the films depending on the deposition conditions. The plot of the hydrogen concentration against the deposition pressures at their preset substrate temperatures are plotted in figure 3.12 below.
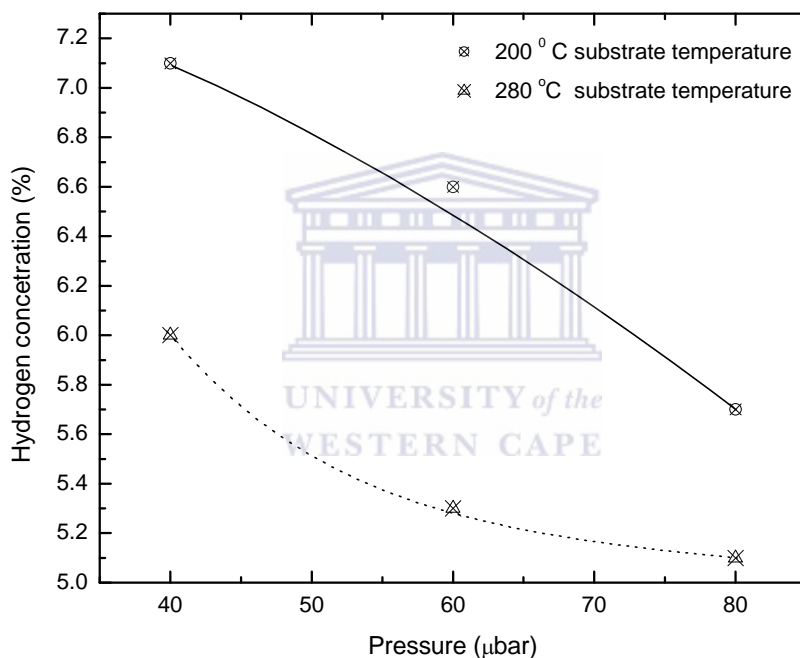
Figure 3.12 The hydrogen concentration of films deposited at their preset substrate temperature and varying pressures.

From the plot in figure 3.12 the hydrogen concentration in the films shows a decreasing trend as both the operational pressure and the substrate temperature are increased. This observation can be attributed to the species reaction on the heated substrate and the nature of the reactions of the radicals on the substrate.

When a series of substrate temperature range studies are done on the growth of a-Si:H, the hydrogen concentration usually show a decreasing trend with increase in the substrate temperature [3.15]. The same pattern is observed in this study, this is because hydrogen diffuses out of the growing film as the substrate temperature is elevated.

The microstructure parameter R^* of the films which can be inferred to as a measure of the void concentration in the films, or the quality of the film, was calculated from the FTIR spectra of the film. The 2100 cm^{-1} and the 2000 cm^{-1} integrated absorption modes were used to calculate the R^* of the films. Figure 3.13 shows the de-convoluted ~2000 cm^{-1} of the a-Si:H film which shows the contribution of the 2100 cm^{-1} mode, which is used in the R^* calculations.
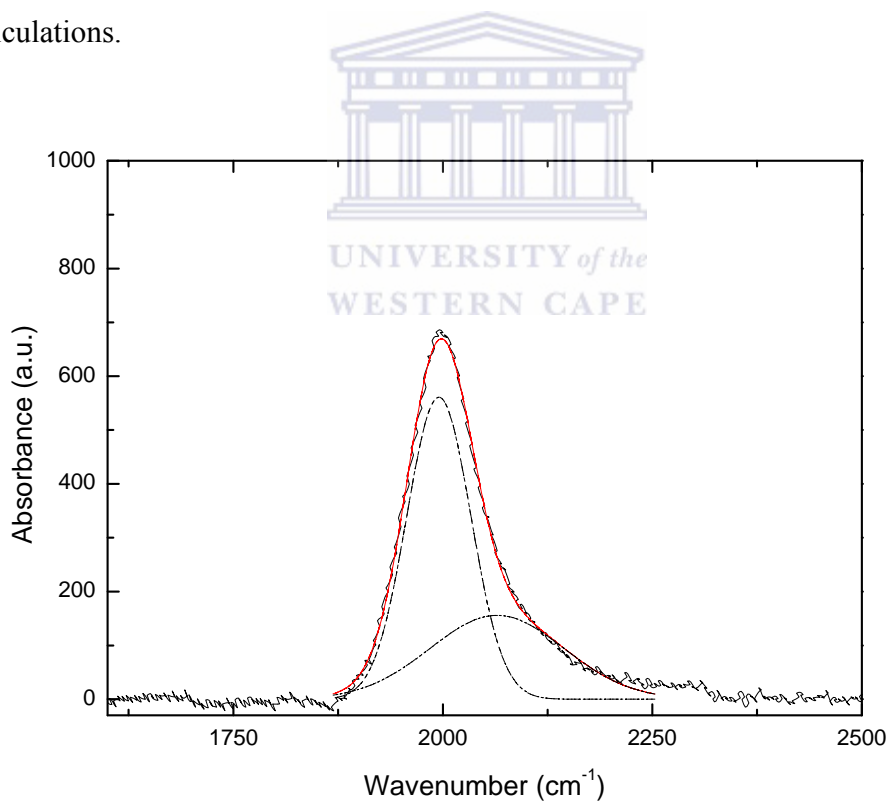
Figure 3.13. The de-convoluted 2000 cm^{-1} mode of the FTIR spectrum of a-Si:H film showing the contribution of the 2100 cm^{-1} mode.

The microstructure parameter R* of the films grown at various deposition conditions are as plotted in figure 3.14.
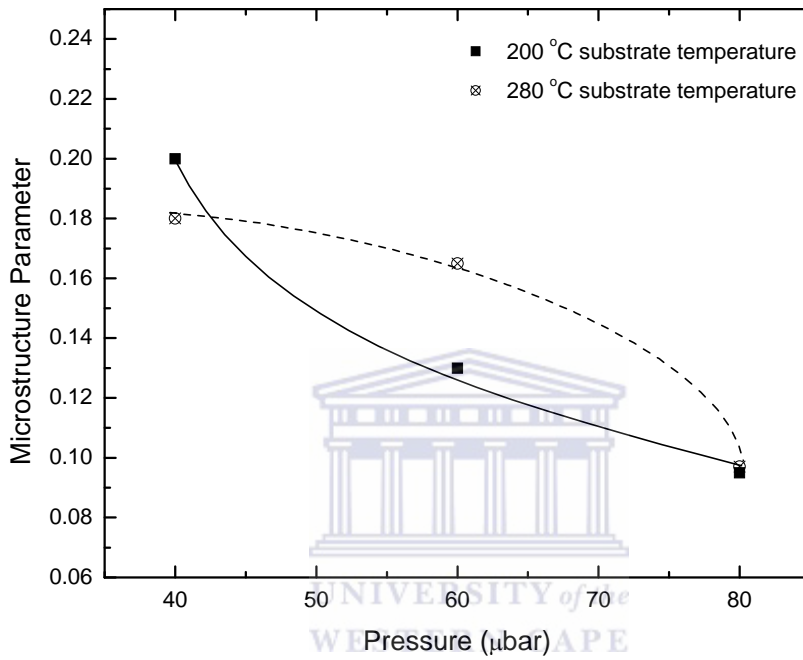
Figure 3.14. Microstructure parameter of the films grown at varying deposition conditions.

The calculation of the R* of the films gives the indication of the dominant bonding configuration in a-Si:H film, this can also used as an empirical determination of the quality of the grown films.

$$R^* = \frac{I_{2100}}{I_{2000} + I_{2100}} \tag{3.2}$$

The plot in figure 3.14 shows that the R* value decreases as the operational pressure and the substrate temperature are increased. This can be interpreted as an improvement in the film structure as the values of the deposition parameters are increased. These results suggest that the Si-H 2000 cm^{-1} mode is the dominant silicon-hydrogen configuration in the grown films. This is because the ~2100 cm^{-1} mode (this mode is only seen when the 2000 cm^{-1} mode is de-convoluted), is not accompanied by the 845 - 890 cm^{-1} (scissors to wagging) mode in the FTIR spectra. The presence of the ~2100 cm^{-1} mode without the 845 - 890 cm^{-1} mode was postulated to be that of Si-H that is located in a microvoid [3.12]. The ratio of the ~2100 cm^{-1} and the ~2000 cm^{-1} from equation 3.2 gives a smaller number, showing that the 2000 cm^{-1} mode has the biggest magnitude. The absence of these higher order silicon hydride FTIR modes (i.e.SiH$_3$ and (SiH$_2$)$_n$ at 845 - 890 cm^{-1}) from the spectra suggests that the a-Si:H film grown is of good quality [3.12, 3.16].

The results of the R* analysis have a similar trend to that observed earlier in the hydrogen concentration analysis, where the hydrogen concentration in the films decreased with the increase in the process pressure and substrate temperature. The lower values of R* from the FTIR analysis serves as an indication that the microvoid density in the films is decreasing as the optimum deposition parameters are reached. This results in more ordered a-Si:H films which are less strained because of the hydrogen incorporation [3.15], and has terminated weak Si-Si bonds by replacing them with Si-H bonds.

3.4 OPTICAL PROPERTIES

3.4.1 Optical band gap

The optical properties of the a-Si:H films were calculated from the transmission spectra of the UV-Vis spectrophotometer. The lack of translational symmetry in a-Si:H film causes it to have a direct band gap.

The optical band gap of the amorphous material was deduced by Tauc [3.17], this is an empirical relation between the absorption coefficient and the band gap in the region of medium absorption. The band gap expression is as shown in equation 3.3

$$(n\alpha h\nu)^{\frac{1}{2}} = \text{constant} \times (h\nu - E_g)\,. \tag{3.3}$$

This relation is used when the mobility edges are assumed to be parabolic in nature. The calculated values of the optical band gap for the films deposited at different set values of operational pressures and substrate temperatures were obtained using the procedure described in section 2.4.

The range of the deposition parameters used to grow films have a direct influence on the Tauc band gap of the a-Si:H films. The variation of the Tauc band gap values with the deposition pressure and the set substrate temperature are plotted in figure 3.15, this clearly shows the evolution of the band gap values. The curves in the plot are for guiding the eye.
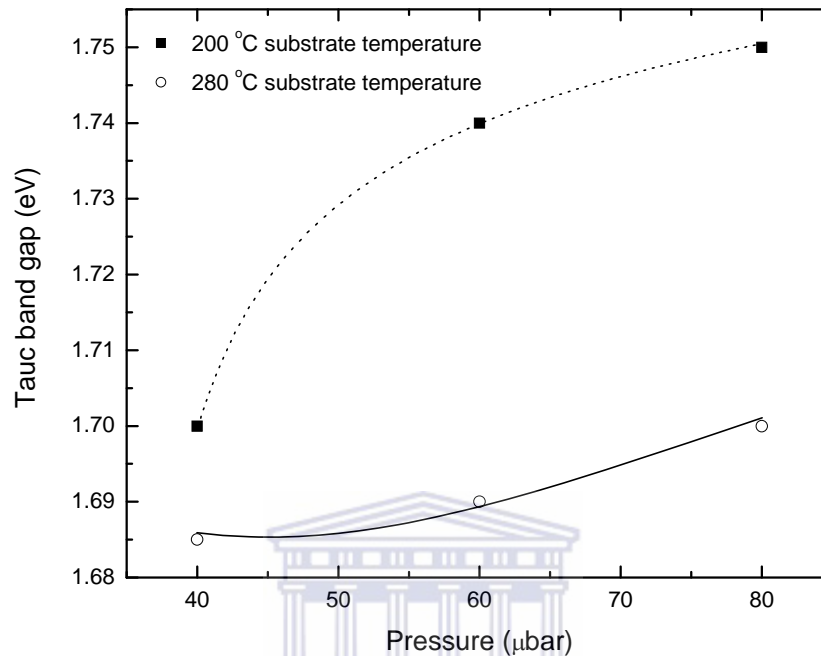
Figure 3.15. The plot of the Tauc band gap versus deposition pressures at 200 $^\circ$C and 280 $^\circ$C substrate temperature.

The band gap of the films shows an upwards trend when the operational pressure is increased from 40 μbar to 80 μbar. However the films deposited at the substrate temperature of 200 $^\circ$C have a greater band gap than those deposited at 280 $^\circ$C. The decrease of the band gap value with an increase in the substrate temperature was also observed in the PECVD prepared films [3.18], and also in the HWCVD work done by Muller [3.15]. One of the contributory factors for this trend was the hydrogen concentration in the films, and this trend was also observed in this study.

The hydrogen concentration can be correlated with the replacement of the Si-Si bonds by the stronger Si-H bonds. This moves the states from the top of the valence band to a position deep within the valence band [3.15]. The microvoids density was postulated as

another cause of the band gap increase [3.19], and from the R[*] study in the FTIR analysis the R[*] values are greatest for films with larger band gap values.

From the XRD analysis of the films, the FWHM of the Gaussian fit of the amorphous hump exhibited a decreasing trend as the operational pressure and the substrate temperature were increased. This was postulated as the improvement of the medium range order, and Raman spectroscopy analysis results of the films grown at the substrate temperature of 280 $^{\circ}$C at various pressures showed better short range order. This suggested that the films have a better tetrahedral structure than those grown at 200 $^{\circ}$C substrate temperature. These observations lead us to believe that the reason the films deposited at 280 $^{\circ}$C substrate temperature have lower band gap values than those grown at 200 $^{\circ}$C is because they have a better tetrahedral structure. (Tetrahedral c-Si has a band gap of 1.1 eV).

From other research group's studies of the band gap of the grown a-Si:H thin films as a function of the substrate temperature during the deposition, it was observed that the band gap of the deposited films decreased as the substrate temperature increases [3.16].

3.4.2 Absorption coefficient

In a-Si:H technology the absorption is determined from the available electronic states only [3.17]. The absorption coefficient of a-Si:H is related to the absorbance by equation 3.4.

$$\alpha = 4\pi \frac{k}{\lambda} \qquad (3.4)$$

The absorption coefficient of a-Si:H films were plotted against the energy of the incident UV-Vis radiation. From the plot in figure 3.16 it is observed that there is a greater

70

absorption coefficient at higher photon energies and this gradually decreases at lower photon energies. This behaviour is normally observed in a-Si:H thin films [3.1, 3.4]. This phenomenon is because when incident photon energies approach the band gap there is no sharp decrease in the absorption due to inherent defects (band tails and mid-gap states) that are common in a-Si:H films.
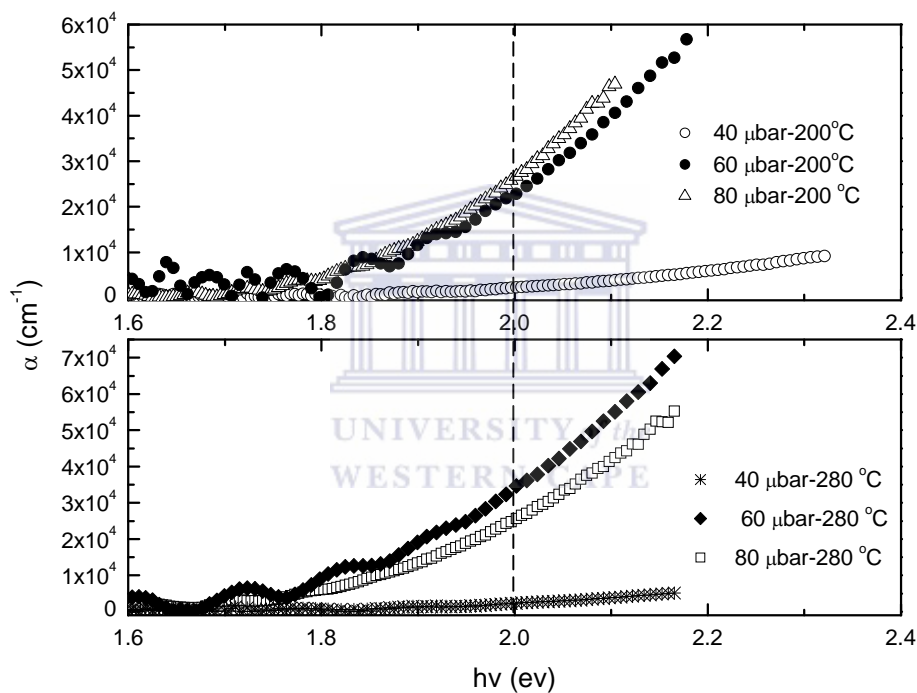
Figure 3.16. The spectra of absorption coefficient versus incident photon energies for the film deposited at different substrate temperatures and varying pressures.

The absorption coefficient at 2 eV (~600 nm wavelength, peak point of the electromagnetic spectrum) for all the films are plotted against the different values of the deposition parameters. This is to show the evolution of the absorption coefficient under varying deposition conditions.
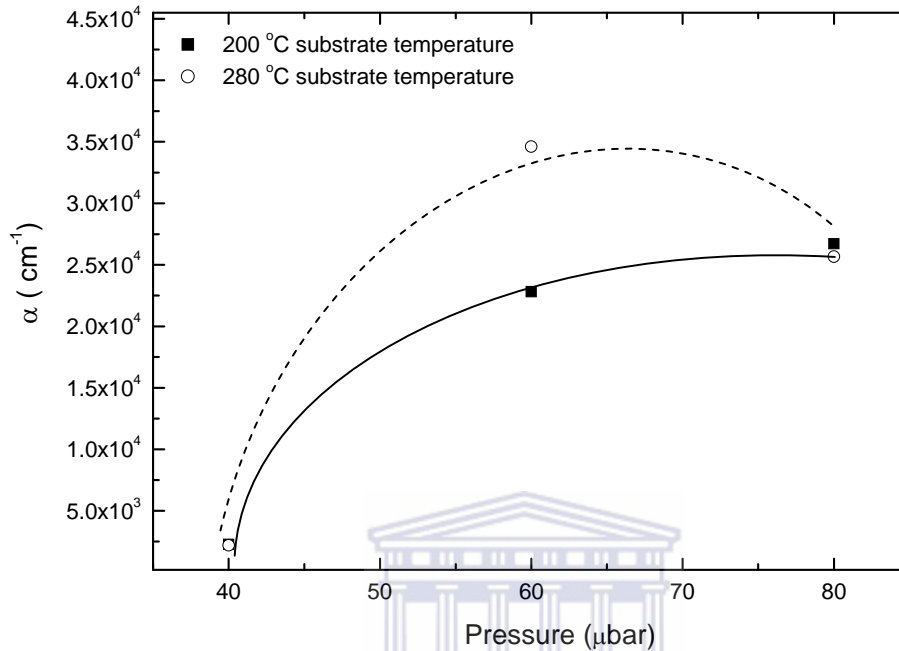
Figure 3.17. Plot of the absorption coefficient at 2eV versus deposition pressure for film grown at 200 ^{o}C and 280 ^{o}C substrate temperatures (curves are to guide the eyes).

It is observed from figure 3.17 that the absorption coefficient of the films deposited at the substrate temperature of 200 ^{o}C increases as the deposition pressure is increased, but for the films deposited at 280 ^{o}C substrate temperature there is an increase in the absorption coefficient when the operational pressure increases from 40 μbar to 60 μbar, and thereafter the absorption coefficient drops such that its value is smaller than that of the film deposited at 200 ^{o}C at 80 μbar. This observation can be interpreted as leading the author to believe that at the substrate temperature of 280 ^{o}C, the 60 μbar operational pressures yield a film with better absorption coefficient.

From similar studies of the absorption coefficient by other groups using the photo-thermal deflection spectroscopy (PDS), the results inferred that the density of defects in the mid-gap states is the lowest for films with high absorption [3.20].

The absorption coefficients of the films grown above the deposition pressures of 40 µbar have values more in the region of the recommended device quality a-Si:H film for solar cell application [3.4].

3.3.3 Refractive index

The refractive index of a-Si:H can be used as an indirect measure of the density of the deposited films [3.2]. Films with very low refractive indices tend to be very porous due to the voids in the film. Hence the refractive index can be used as an approximate indicator of the quality of the deposited films. The refractive indices of the films were calculated at zero energy (n_0) using the procedure described in section 2.4.

The refractive index of a-Si:H at zero energy ranges between 2.9 and 3.14 [3.21] whereby the films with upper edge of n_0 are desirable because the refractive index of the film leans more closely to that of single crystalline silicon i.e.3.42.
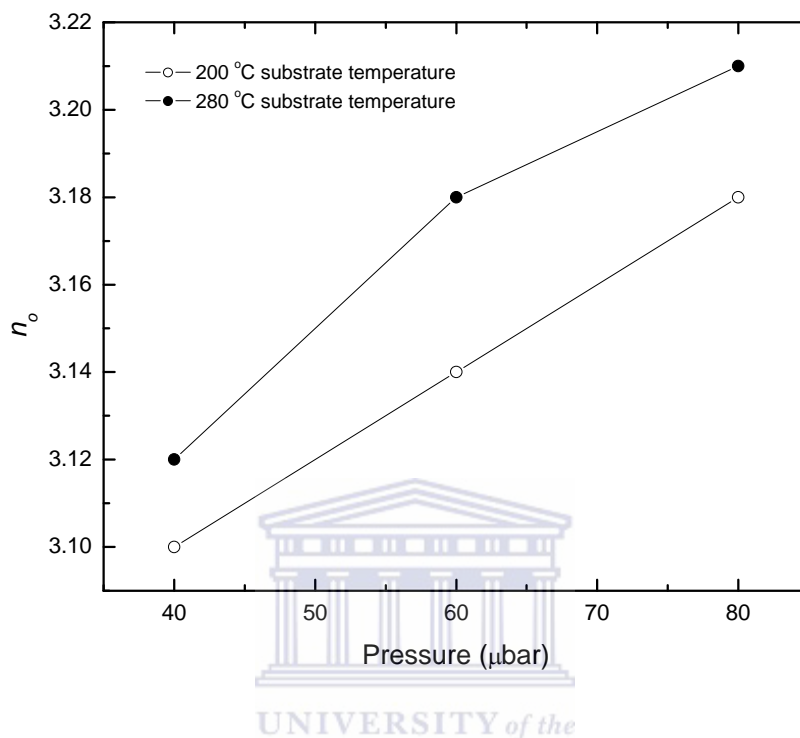
Figure 3.18. Plot of the refractive index versus the deposition pressure at zero energy at 200 $^{\circ}$C and 280 $^{\circ}$C substrate temperature.

From the plot in figure 3.18 it is observed that the refractive indices of the films deposited at 200 $^{\circ}$C and 280 $^{\circ}$C substrate temperatures increases as the operational pressure increases. The films grown at the substrate temperature of 280 $^{\circ}$C show as more compact and ordered because of the higher magnitude of the refractive index. Hence the films grown at 280 $^{\circ}$C substrate temperature and elevated pressure have a structure more tetrahedral hence these films have a denser a-Si:H network.

The improvement of the refractive index with the increasing substrate temperature can be explained by the fact that, at higher substrate temperature the molecules arriving at the substrate surface have a higher kinetic energy. This enables them to move in search of a better site with higher electro-negativity, with the possibility of displacing hydrogen from

the surface. This results in a decrease in hydrogen incorporation and densification of the growing film [3.2, 3.15].

The FWHM of the Gaussian fit of the amorphous hump on the XRD spectra, showed that the medium range order of the films improve as the deposition pressure and the substrate temperature increases towards the optimum. The angular disorder $\Delta\theta_b$ of the films calculated from the width of the *TO* mode on the Raman spectroscopy data, also showed an improvement of the short range order in the films as the pressure and the substrate temperature increases.

The refractive index results show an agreement with the structural analysis of the film from the XRD and Raman spectroscopy.

3.5 Summary

The summary of the results of all the analytical techniques used to characterize the intrinsic film will be linked together to give a bird's eye overview of the analysed results at a glance. In table 3.2 all the results of the different analysis techniques are given with the set values of the deposition parameters.

Table 3.2 Analytical techniques results and the preset values of the deposition conditions.

Deposition Conditions	XRD FWHM	Raman $\Delta\theta_b$	Band gap(eV)	α at (cm^{-1})	Refra index	FTIR H%	FTIR R*
40 µbar – 200 °C	3.90 °	7.0 °	1.70	2281	3.10	7.1	0.200
60 µbar – 200 °C	3.70 °	6.38 °	1.74	22819	3.14	6.6	0.130
80 µbar – 200 °C	3.65 °	5.7 °	1.75	26706	3.18	5.7	0.095
40 µbar – 280 °C	3.80 °	6.8 °	1.67	2200	3.12	6.0	0.180
60 µbar – 280 °C	3.75 °	6.2 °	1.69	34609	3.18	5.3	0.160
80 µbar – 280 °C	3.60 °	5.6 °	1.70	25668	3.20	5.1	0.096

From table 3.2 it is observed that the FWHM at ~28 ° from XRD spectra of the films decreases as the operational pressure increases. The 40 µbar films exhibit larger values of FWHM which means these films do not possess a good medium range order.

The $\Delta\theta_b$ of the films shows improvement as the operational pressures and substrate temperatures set values are increased and this suggest that the films short range order gets better at these elevated values of the deposition parameters. The refractive indices of the films also show a trend similar to that of $\Delta\theta_b$ at the elevated set values of the deposition parameters. The films deposited under these conditions have the lowest values of the microstructure factor, which suggest that the films have a low concentration of microvoids.

The hydrogen concentration of the films also decreases as the deposition conditions are set at higher substrate temperatures and pressures and the band gap of the films also approaches a device quality magnitude recommended in literature [3.11] for solar cell application.

From the trend that is observed from the analysed results of the films, the optimum regime for the growth of good quality a-Si:H film in this study is achieved at operational pressures greater than 40 μbar and the substrate temperature set at the elevated temperature.

These set of the optimum deposition conditions (*280 ^{o}C and 80 μbar*) will be used to grow n-type films by diluting PH_3 in SiH_4 gas in varying concentrations, this will be achieved by setting the flow rate of the gases at desired flow rate ratios. Similarly for p-type film these optimum conditions will be used.

References:

[3.1] R.A. Street, *Hydrogenated amorphous silicon, Cambridge University Press* (1991).

[3.2] K.F. Feenstra, *Hot-wire chemical vapour deposition of amorphous silicon and the application in solar cells*, Ph.D thesis, Utrecht University , 1998.

[3.3] Q.Wang, E. Iwaniczko, Y. Yang, K. Lord, S. Guha, K. Wang, D. Han, 29th IEEE P.V. Specialist conference.

[3.4] R.E.I. Schropp and M. Zeman, *Amorphous and microcrystalline silicon solar cell: Modeling, Materials and Device Technology*, Kluwer Academic Publisher (1998).

[3.5] K.F. Feenstra, R.E. Schropp, W.F. van Weg, J. Appl. Phys. **79** 2699 (1996).

[3.6] A.H. Mahan, J. Yang, S. Guha, D.L. Williamson, Mater. Res. Symp. Proc **557** 296 (1996).

[3.7] A.H. Mahan, D.L. Williamson, T.E. Furtak, Mater. Res. Symp. Proc. **467** 657 (1997)

[3.8] D.L. Willianson, Mater. Res. Symp. Proc. **557** 251 (1991)

[3.9] H. Touir, J.F. Morhange, j. Dixie, Soli State Communication **110** 315 (1999)

[3.10] M. Konagai, T. Tsushima, M.K. Kim, K. Asakusa, A. Yamada, Y. Kudriavtsev, A. Villegas, R. Asomoza, *Thin Solid Films* **395** 152-156 (2001).

[3.11] J.K. Holt, M.Swiatek, D.G. Goodwin, R.P. Muller, W.A. Goddard III, H.A. Atwater. Thin Solid Film **395** 29 -35 (2001).

[3.12] Properties of Amorphous Silicon and it's Alloys, **2.1** A.H. Mahan, *Structural information on a-Si:H from IR and Raman spectrometry*. Edited by Tim Searle. An INSPEC Publication, Emis Data Review Series **19** ISBN 08529699228.

[3.13] A.J.M. Bernstern, Structural Disorder in pure and hydrogenated amorphous silicon (Ph.D thesis), niversityof Utrecht, the Netherlands (1993)

[3.14] D. Beeman, R. Tsu, M.F. Thorpe, Physical. Review. **B32** 874 (1985).

[3.15] T.F.G. Muller, M.Sc thesis, *Crystallization of amorphous silicon thin films at elevated temparetur*e, University of the Western Cape, 2002.

References:

[3.16] Properties of Amorphous Silicon and it's Alloys, **2.3** M.Stutzmann, Data on hydrogen in a-Si:H from the IR and Raman spectroscopy. Edited by Tim Searle. An INSPEC Publication, Emis Data Review Series **19** ISBN 08529699228.

[3.17] J. Tauc, Optical Properties of Solids, edited by F. Abeles (North-Holland, Amsterdam, the Netherlands) 277 (1972).

[3.18] H. Meiling, Ph.D. Thesis, Utrecht University, Utrecht, the Netherlands, (1991)

[3.19] S.R. Jadkar, J.V. Sali, S.T. Kshirsagar, M.G. Takwale, *Solar Energy Materials & Solar cell* **85** 301 – 312 (2005).

[3.20] M. Daouahi, A. Ben Otmane, Z. Zellama, A. Zeitnert, M. Essaret, H. Bouchriha, Solid State Comm. **12** 243 (2001)

[3.21] S.Halidintwali. *A study of hydrogenated nanocrystalline silicon thin films deposited by Hot-Wire Chemical Vapour Deposition (HWVCD)*, Ph.D thesis. Univeristy of the Western Cape. Bellville
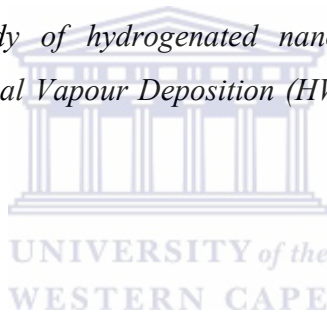
Chapter 4

4.1 DOPING

4.1.1 Introduction

After the experimental evidence that showed that hydrogenated amorphous silicon (a-Si:H) can be doped both n-type and p-type [4.1], the interest in the field of a-Si:H technology increased. This lead to a fabrication of devices based on the a-Si:H technology. The fabrication of devices comes with a need to understand the structural, optical and electrical properties of the doped a-Si:H.

Doping in a-Si:H by group 3B and 5B elements result in a shift in Fermi level of the material [4.2]. This (doping) also has an effect on the matrix network and produces bulk and surface effects [4.2-4.3]. The dopant atoms can exist either in the inactive or electronically active state in the a-Si:H matrix depending on the coordination of the dopant atoms [4.4].

For the study of n-type doping of a-Si:H, phosphorous (P) was chosen as a dopant element. Phosphorous was obtained from the fragmentation of phosphine gas (PH_3) when it interacted with a heated tantalum wire in the HWCVD chamber.

For device application the quality of the n-type film is important because this layer forms part of the window layer in the n-i-p cell structure. This film helps in creating the electric field that drifts the charged carriers in the photovoltaic process. The optimum deposition regime is required to produce a good quality n-type film for solar cell application. The deposition parameters and values used to grow the n-type film are as shown in table 3.3 below. (The values of the deposition parameters were chosen such that they are in the expected range of good quality films this is based on preliminary

work done in the research group).

Table 4.1 Deposition conditions of the n-layer grown in the HWCVD chamber.

Deposition parameter	Values
Filament temperature	1800 ^{o}C
Substrate temperature	280 ^{o}C
Silane flow rate	49 - 43 sccm
Phosphine flow rate	1 - 7 sccm
Pressure	60 μbar and 80 μbar

4.1.2 XRD spectroscopy
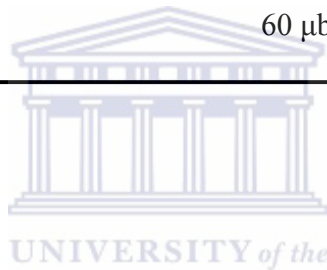
The n-type films were deposited using the values on table 4.1 of the deposition parameters. The deposited films were grown such that the thicknesses of the films were approximately the same (~1 μm) as recommended for the analysis of the amorphous films [4.5]. The microstructures of the grown films were characterized using the XRD spectroscopy technique. All the XRD spectra in this section were substrate subtracted as described in chapter 3.

The microstructure results of the films as determined from the XRD spectroscopy show that the films have an amorphous nature, figure 4.1 shows the XRD spectra of all the films with the hump which is a characteristic of amorphous material. The XRD spectra of the films show a slight shift of the amorphous hump, which is now centered around ~26°, rather than the usual ~28° seen in intrinsic amorphous film.

This hump is due to the lack of long range order in this class of materials, and hence there is no periodic repeat of the unit structure. This nature of amorphous material makes it impossible to satisfy Bragg's condition because there is no constructive inference on diffracted incident x-ray radiation [4.6].
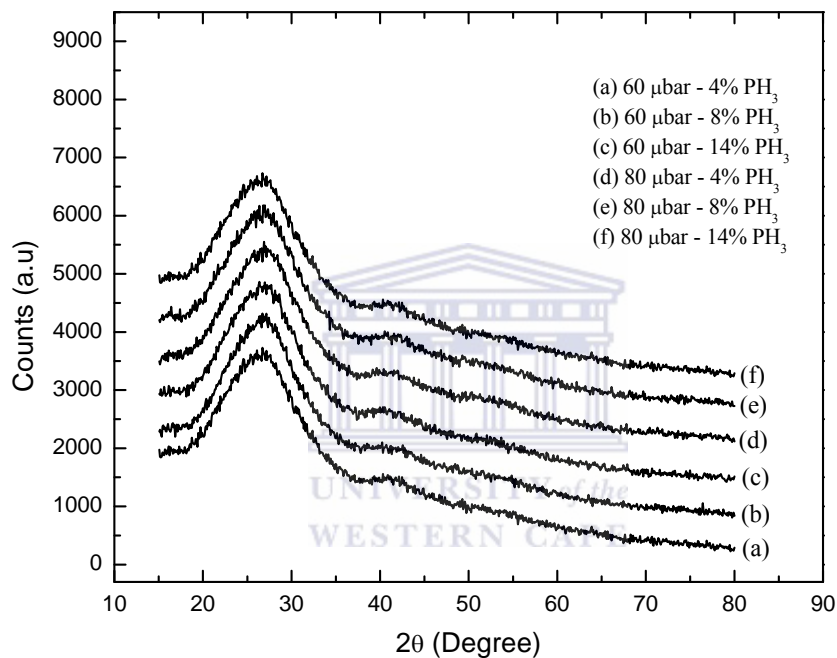
Figure 4.1. XRD spectra of percentage PH_3 at varying pressures and 280 ^{o}C substrate temperature.

The FWHM of the Gaussian fit of the films was calculated at ~26° to determine the medium range order of the doped films. The values were found to be between 4° and 4.1^o, this broadening in the amorphous hump increased with the PH_3 percentage in the gas phase. From literature it is known that the addition of dopants in the a-Si:H network increases the network disorder [4.2, 4.4], hence the greater degree of broadening of the amorphous hump for the n-type film as function percentage PH_3. A comparison between the medium range order of the intrinsic films in section 3.2.2 and that of the doped films

82

show that doping increases the disorder in the films. From this result it can be said that the structural ordering on a length larger than the nearest neighbour in the doped a-Si:H, exhibit a deviation from the tetrahedral structure of silicon that is more pronounced because of doping [4.7-4.9].

4.1.3 Raman spectroscopy

Raman spectroscopy can be used to determine the short range order of the amorphous films. This is determined from the evolution of the FWHM of the *TO* mode [4.10] in grown films. The root-mean-square bond angle variation ($\Delta\theta_b$) is used to quantify the short range order in the films. The entire series of n-doped samples showed no sign of a Raman 520 cm^{-1} shift which is due to the presence of the crystallites in the films. The spectrum in figure 4.2 is representative of all the samples because they were all shown to have an amorphous nature.
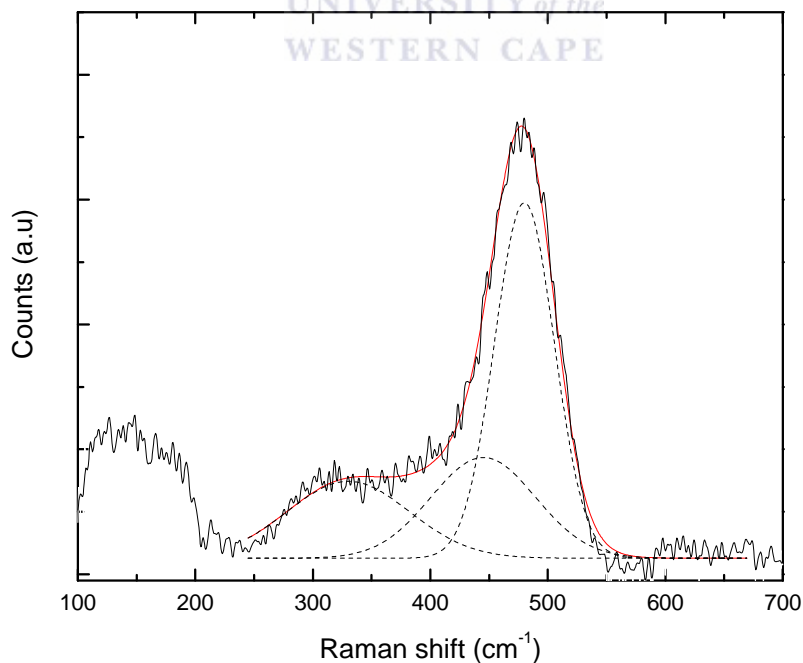

Figure 4.2. A representative spectrum of the Raman shift spectrometry of n-type films.

The FWHM of the *TO* mode (480 cm^{-1}) of the Raman spectra were used to calculate the $\Delta\theta_b$ of the n-type films. The calculations of the $\Delta\theta_b$ were done for all the films with various PH$_3$ percentage dilutions in the silane gas during deposition at the range of values of the operational pressure.

The plot in figure 4.3 shows how the $\Delta\theta_b$ changes with the PH$_3$ percentage dilution in silane during the growth of the n-doped film.
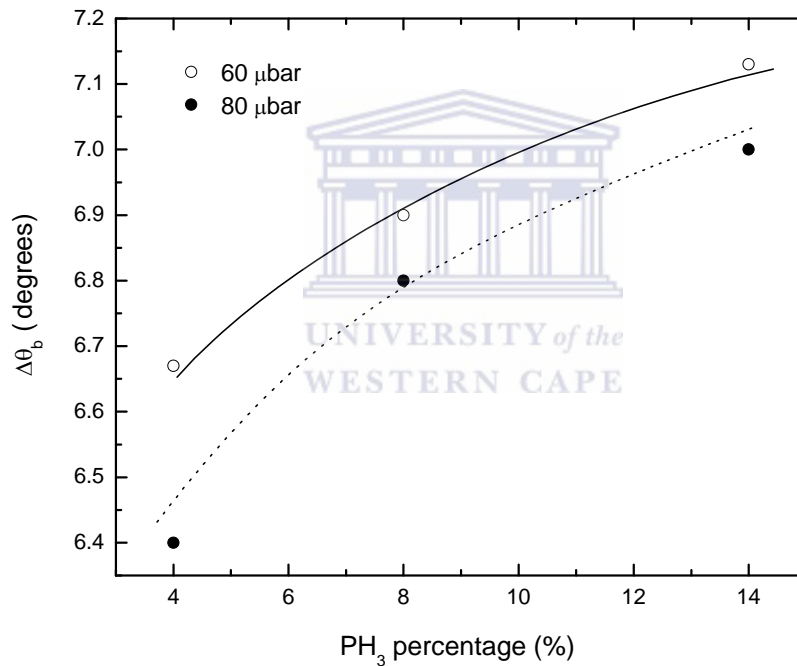
Figure 4.3. Plot of $\Delta\theta_b$ against the percentage PH$_3$ at different operational pressures (curves on the plot are to the eyes).

This observation is as expected because it is known that doping of a-Si:H increases the density of defects in the a-Si:H films [4.4], hence the deterioration in the short range order of the films as shown from the plot in figure 4.3. The bond angles of these films deviate from the tetrahedral shape with the PH$_3$ percentage in the gas phase. These results

substantiate the trend seen from the XRD analysis, whereby the FWHM of the Gaussian on the amorphous hump was broadening with the percentage of PH_3.

4.2 OPTICAL CHARACTERIZATION

The grown films were analyzed for optical properties using the transmission spectra of the UV-Vis spectrophotometer. The a-SiP:H film was grown by diluting phosphine gas in silane, and then flowing it into the reaction chamber. The grown films were only slightly doped with phosphorous from the phosphine gas, this resulted in films that are not alloyed but only have small amounts of phosphorus bonded to silicon atoms in the a-Si:H matrix. The introduction of the dopant in a-Si:H alters the electronic states of silicon in a-Si:H by shifting the Fermi level towards the mobility edge [4.4, 4.8].

4.2.1 Absorption coefficient

The absorption coefficient of the n-type film is important in an n-i-p cell structure, since photons from the sun enter the device through this layer. The absorption coefficient of the n-layer should be such that the photon energy is not parasitically absorbed by this layer, but sufficient photons should also reach the intrinsic and p-doped layers in the process. The absorption coefficient of the n-layer was calculated using the mathematical procedure explained in section 2.4.

The plots of the absorption coefficients of the films deposited at varying conditions versus incident photon energy are shown in figure 4.3. The data from the figure 4.3 plot shows the absorption coefficient of the films as a function of the percentage of PH_3 in the gas phase. The absorption coefficients of all the films were compared at 2 eV photon energy, which is where the solar radiation peaks.
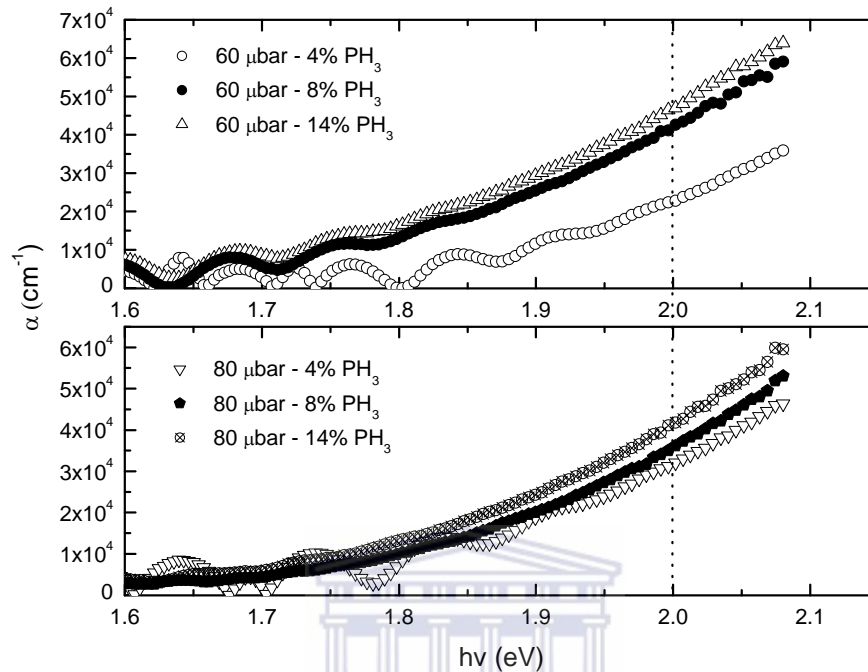
Figure 4.3. Plot of absorption coefficient against incident photon energy.

The absorption coefficients of the films show high values at higher photon energies as observed from the plots in figure 4.3. The absorption coefficient does not decrease sharply when the photon energies approach the optical energy gap. This is because of the inherent defects in doped a-Si:H films, which introduces midgap electronic states and band tails.

The defects in the films are due to the distorted bond lengths and bond angles that deviate from the ideal silicon tetrahedral structure [4.4, 4.10]. The inclusion of the phosphorous atoms could also affect the local structure because of the mismatch in the size of the atomic radius compared to other silicon atoms. The angular disorder ($\Delta\theta_b$) of the films was shown by Raman spectroscopy results to be greater than those of the intrinsic films. The graph of the absorption coefficients of the films (at 2 eV) against the percentage PH_3 ranges of values of operational pressures are plotted in figure 4.4.

This is to show the effect that the percentage of PH_3 has on the absorption coefficient.
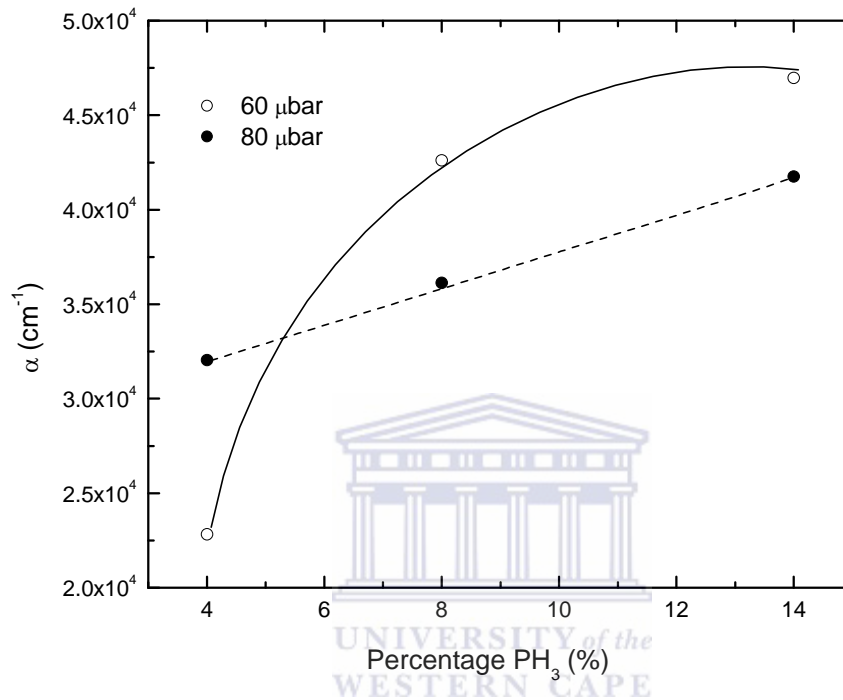
Figure 4.4. The plot of absorption coefficient at 2 eV of the films at varying values of pressure and percentage PH_3. (curves on the plot are to the eyes)

From the plot in figure 4.4 it is observed that the absorption coefficient of the films at 2 eV increases as the percentage of PH_3 diluted in silane increases. This phenomenon could be due to the defects in the mid-band gap states that dopant atoms are known to create [4.4]. The range of the absorption coefficient from this study are comparable with those seen in other studies done elsewere [4.11]. The films grown at the operational pressure of 60 µbar shows a better absorption coefficient.

4.2.3 Optical band gap

The optical band gap of the doped films was deduced from the empirical relation presented by Tauc as presented in section 3.1. The transmission spectrum from the UV-Vis spectrophotometer was used in calculating these optical parameters.
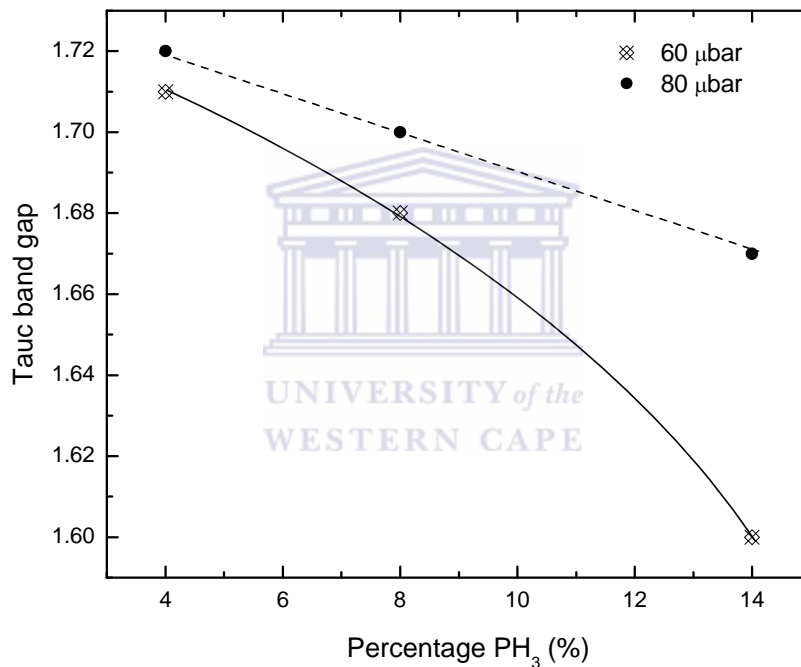
Figure 4.5. The plot of Tauc band gap of the films versus percentage PH₃ grown at different operational pressures. (Curves on the plot are to guide the eyes)

The Tauc band gap of the doped films deposited at various set values of the deposition parameters are plotted in figure 4.5, this is to show how the Tauc band gap evolves as the deposition parameters are changed. The Tauc band gap shows a decreasing trend with increases in the percentage of PH₃ for the films deposited at their operational pressure.

Aken et.al [4.11] observed the same behaviour when a-Si:H was n-doped. The optical band gap of the n-type films exhibit a decreasing trend as the percentage PH_3 increase, this trend is contrary to the behaviour observed in the optical gap of the intrinsic films. This could be attributed to the dopants shifting the Fermi level in the density of state of the films. The values of the band gap calculated closely agree with the recommended values from literature [4.4].

4.3 ELECTRICAL CHAARATERIZATION

The Hall Effect measurements were performed on these n-type doped films to determine the electrical properties of these films. The carrier concentration of the films increased with the percentage PH_3 that is diluted with silane in the reaction chamber.
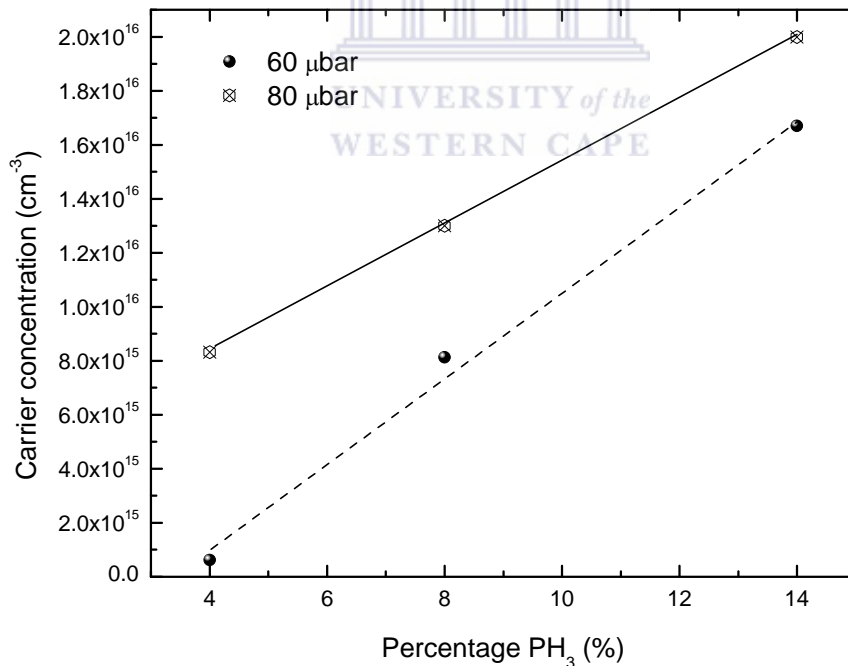
Figure 4.6. The plot of active carrier concentration in the deposited film versus percentage PH_3 at varying operational pressures.

89

Figure 4.6 shows the number of active carriers in the doped films grown using different deposition conditions for solar cell application. From the plot in figure 4.6 it is observed that the active carrier concentration from the Hall Effect measurements increase with the increasing percentage of PH_3 in the gas phase reaction. This trend is similar to the one exhibited by the dark conductivity measurement on the samples in figure 4.7 which shows the plot of dark conductivity versus the operational pressure.
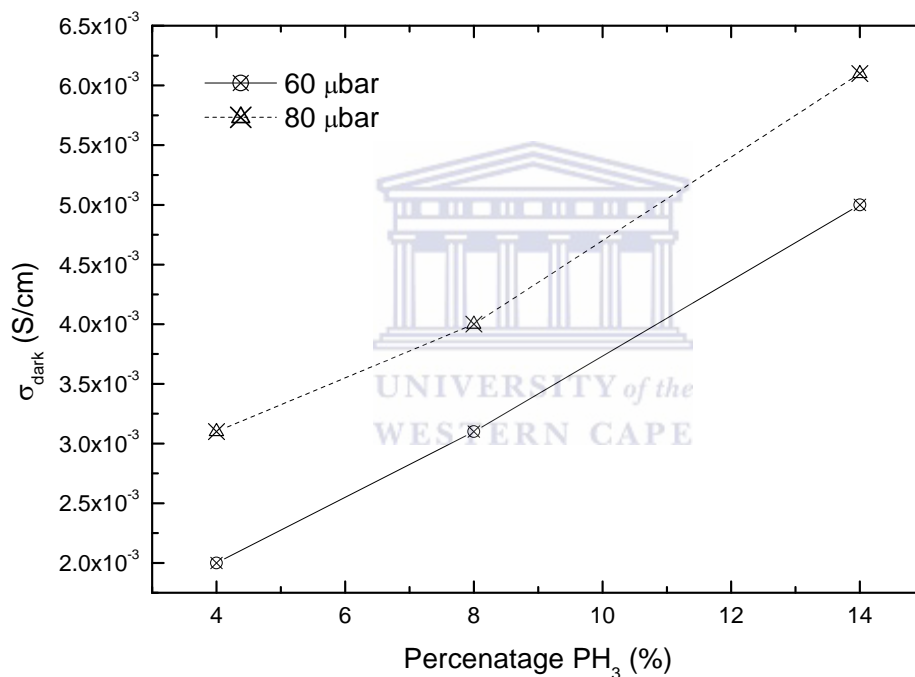
Figure 4.7. The plot of dark conductivity in the films versus the percentage PH_3 at varying operational pressures.

This similarity in the trend of carrier concentration and dark conductivity measurements can be ascribed to the fact that the electrons from the donor phosphorous are the entities that contribute to these physical measurements. From the electrical measurements it is evident that the a-Si:H is successfully doped.

4.4 SUMMARY OF n-TYPE

The summary of the results of all the analytical techniques used to characterize the n-type films are linked together to give an overview of the analysis results at a glance. In table 4.2 all the results of the different analytical characterization are given with the set values of the deposition parameters.

Table 4.2 Summary of all the analytical results of the n-type film

Deposition Conditions	XRD FWHM	Raman $\Delta\theta_b$	Band gap (eV)	α (cm^{-1}) at 2eV	Carrier concentration	Dark conductivity
60 µbar – 4% PH$_3$	4.0 ^{o}	6.6 ^{o}	1.71	22819	6.2×10^{14}	2.0×10^{-3}
60 µbar – 8% PH$_3$	4.1 ^{o}	6.9 ^{o}	1.68	42607	8.0×10^{15}	3.1×10^{-3}
60 µbar – 14% PH$_3$	4.2 ^{o}	7.2 ^{o}	1.60	46970	1.6×10^{16}	4.0×10^{-3}
80 µbar – 4% PH$_3$	4.0 ^{o}	6.4 ^{o}	1.72	32038	7.8×10^{15}	3.3×10^{-3}
80 µbar – 8% PH$_3$	4.1 ^{o}	6.8 ^{o}	1.70	36136	1.2×10^{16}	4.1×10^{-3}
80µbar - 14% PH$_3$	4.1 ^{o}	7.0 ^{o}	1.68	41726	2.0×10^{16}	6.0×10^{-3}

The XRD FWHM of the n-type films is greater than those of the intrinsic films in section 3.2.2. This accords with the fact that impurities in the a-Si:H increases the disorder of the growing film. Even the short range order of the film is slightly greater compared to that of the intrinsic a-Si:H film, as observed from the Raman $\Delta\theta_b$.

The introduction of these n-type dopants increases the carrier concentration in the n-type film and this carrier concentration increases with the PH$_3$ percentage in the gas phase. The results from the Hall Effect and the dark conductivity measurements show that the values obtained from the measurement are close to those in literature. The introduction of dopant atoms in the a-Si:H network successfully doped the films as is evident from the structural, electrical and optical measurements.

4.5. P-TYPE DOPED a-Si:H

4.5.1 Introduction

P-type films of a-Si:H are generally grown by doping a-Si:H with group 3B elements of the periodic table. This is because atoms of group 3B elements have three valence electrons which when they bond with silicon in a-Si:H material holes are created. Commonly used p-type dopant feedstock gas in the HWCVD technology is diborane (B_2H_6). The p-type films can either be grown as amorphous or nano-crystalline depending on the values of the experimental parameters. a-Si:H can also be grown as polycrystalline using other techniques where the crystallization is induced by a metal layer and results in a polycrystalline film that is p-type.

4.5.2 Metal Induced Crystallization (MIC)

The metal induced crystallization (MIC) of the a-Si:H has been regarded as a promising technology for low-temperature fabrication of large area polycrystalline silicon (poli-Si) with a larger grain size, for photovoltaic application [4.12 - 4.13]. The MIC process has been a alternate process for solid phase or laser crystallization of a-Si:H [4.14]. This process of metal induced crystallization (MIC) has been dubbed as an economically attractive way of producing poly-Si with larger grain sizes at a low annealing temperature (<450 ^{o}C) in a short time [4.15]. In the MIC a thin film of a metal is deposited on a film of a-Si:H, then heated in a furnace to induce crystallization of a-Si:H to a polycrystalline film.

The crystallization of the films from the Si/metal system can be divided into two categories, (i) a simple eutectic system like Si/Al that does not form any silicides when used for the crystallization of a-Si:H, and (ii) compound forming systems like Si/Ni, which form silicides [4.16]

There have been some advances in the metal induced crystallization process whereby the aluminium-induced crystallization layer exchange (ALILE) process was developed [4.17]. This resulted in a glass/poly-Si/Al(Si) structure from a stacked glass/Al/a-Si with a (100) preferential orientation. Different metals have been used for the MIC process [4.18 - 4.21] but aluminium (Al) has been found to be a promising metal for the crystallization process in photovoltaic applications because films prepared in this way produce p-type materials with a desirable hole concentration as measured by Hall Effect analyses[4.22].

4.5.3 Aluminium Induced Crystallization P-Doping (AICPD)

For this study the p-doped films of a-Si:H were grown by doping the a-Si:H with evaporated aluminium in the reaction chamber instead of the traditional dopant gases or MIC process. The growth of a-SiAl:H was achieved by co-deposition of a-Si:H and aluminium in the HWCVD reaction chamber and allowing the species to react on their way to the heated substrate and also on the substrate. This deposition process is a combination of a *physical evaporation* of aluminium and *HW-chemical vapour deposition* in a one step deposition of p-doped film.

The silicon hydrides from the fragmented SiH_4 on the hot wire react with the physically evaporated aluminium atoms. The assumption is that aluminium reacts with the silicon hydrogen radicals in the gas phase to promote doping, and that there are also reactions on the heated substrate when the species coalesce and agglomerate to form a p-type film.

The deposition conditions of the intrinsic film that showed better structural and optical properties were used in the growth of the p-doped layer. The only variable that was introduced in the deposition condition is the physical evaporation of the aluminium in the reaction chamber.

4.5.4 Energy dispersive x-ray spectroscopy (EDS)

The aluminium concentration that is incorporated in the grown films was determined by energy dispersive x-ray spectroscopy (EDS) in the scanning electron microscope (SEM). The aluminium percentage incorporated in the prepared film was found to be approximately 4 at %. Figure 4.23 show the EDS spectrum of the probed p-type film.
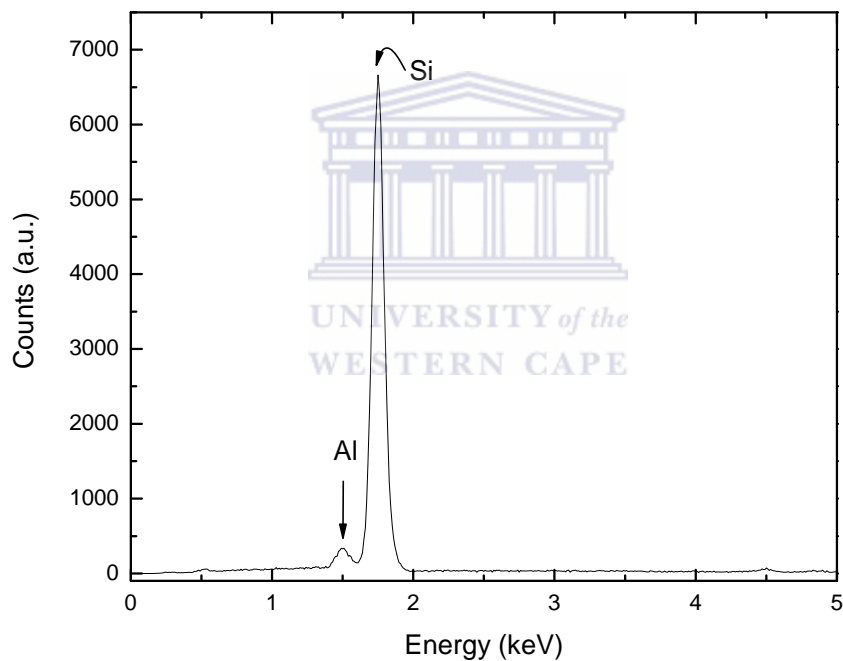
Figure 4.23 EDX spectrum of the a-SiAl:H showing the aluminium and silicon peaks. (This is a representative spectrum of all the films).

4.5.5 XRD spectroscopy

The microstructure of the p-doped films was determined by XRD spectroscopy, and from the typical XRD spectrum as in figure 4.24 the grown films are shown to be poly-crystalline in their atomic arrangement. This resembles the microstructure that results when a-Si:H thin films are crystallized when a thin layer of aluminium is evaporated

on the a-Si:H thin film, and annealed at elevated temperatures in the evacuated furnace for some time. The result from the XRD spectroscopy suggests that the process of aluminium induced crystallization (AIC) was achieved by a single step process. This was achieved when radicals from the fragmented silane reacted with physically evaporated aluminium during the growth of the p-doped layer.
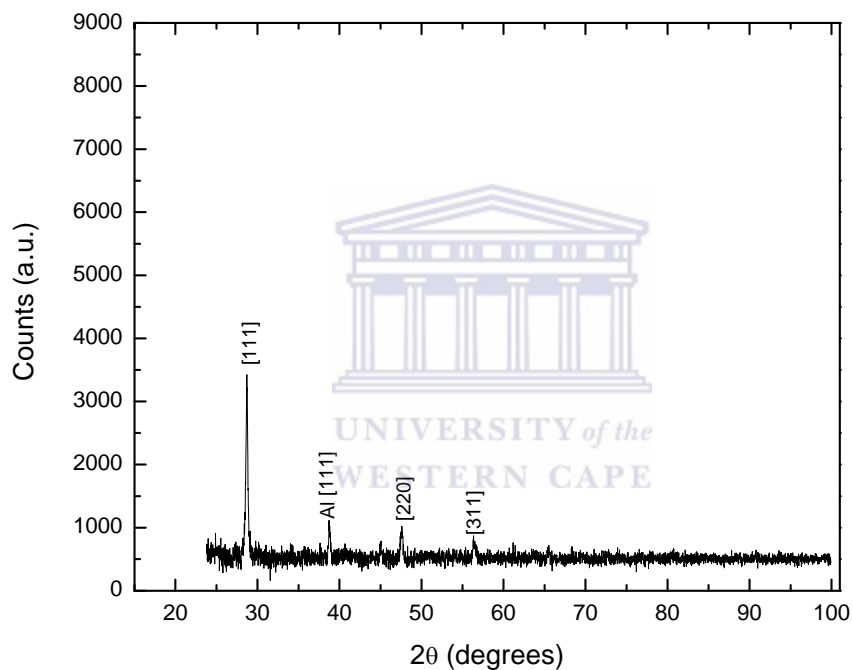
Figure 4.24 XRD spectrum of the aluminium p-type doped film. (This is a representative spectrum of all the films).

The spectrum of p-doped films in figure 4.24 leads to the suggestion that the reaction between silicon hydrides radicals and aluminium vapour in the gas phase and on the substrate, has the same effect as all the steps of the AIC process combined. This is suggested because of the polycrystalline phase as shown from the XRD spectra. This XRD spectrum clearly shows the [111], [220] and [311] sharp peaks of a polycrystalline

silicon. From this XRD spectrum it can be clearly seen that there is no amorphous contribution to the spectrum, therefore the crystallization took place throughout the bulk of the film during growth.

In the next section of this work it will be shown that this polycrystalline film is also p-doped, since the solar cell device manufactured using this single step reaction process to grow a p-dope film at the same time inducing crystallization, gave a fully functional solar cell device.

It should be borne in mind that *aluminium induced crystallization p-doped* (*AICPD*) films were grown at the substrate temperature of 280 ^{o}C and this substrate temperature is well below the temperature required to induce crystallization of a-Si:H by aluminium induced reaction (AIC) in a solid phase reaction.

This single step reaction of *the aluminium induced crystallization p-doped* (*AICPD*) reaction will be used to grow a p-doped layer for solar cell device application.

4.5.6 Rutherford Backscattering Spectrometry (RBS)

The thermal stability of the p-doped film was investigated using RBS spectrometry and this was done to check if there is any migration of aluminium in the film when this film's substrate is heated during the manufacturing of the solar cell. The real time RBS spectrometry set-up was used for this measurement. In this set-up a sample of p-doped film is mounted on a substrate heater in the RBS chamber. The sample is then in-situ annealed from room temperature to 380 ^{o}C at a ramp rate of 3°/min, this happens while the He^{2+} particles are targeted on the sample for the RBS analysis. The annealing temperature of 380 ^{o}C was chosen because the maximum substrate temperature range for the growth of the films in this study was 280 ^{o}C and this is 100 ^{o}C clear of the deposition substrate temperature.

In this experimental set up the interaction takes place between the p-doped film atoms and the He^{2+} particles while the film is being annealed. The data from the backscattered He^{2+} at the detector is captured in real time.

The RBS spectrometry spectra in figure 4.25 show that there is no migration of aluminium in the film during the in-situ annealing of the sample. The peak that is due to the contribution of aluminium and silicon species in the p-doped film on the RBS spectra shows no signs of energy shift and this suggests that there is no migration of the aluminium in the film. The energy and the channel number of the aluminium remains the same throughout the annealing process. This film proves to be thermally stable when heated at these elevated substrate temperatures, therefore the aluminium species in the *AICPD* film will not migrate into the intrinsic layer in the n-i-p cell configuration during the manufacturing of the cell.

These results are contrary to what is observed in the MIC process. In the MIC process the aluminium atoms diffuse into the a-Si:H in order to induce crystallization of the film [4.13]. The same phenomenon of diffusion of aluminium was also observed in the ALILE process, here the aluminium even migrated through the a-Si:H while crystallizing it [4.14]. Other research groups even observed aluminium diffusion into the a-Si:H at temperatures lower than 380 ^{o}C. The *AICPD* films grown in this study have the aluminium atoms tightly bonded to the silicon matrix, hence there is no migration of aluminium species during the annealing of the film.
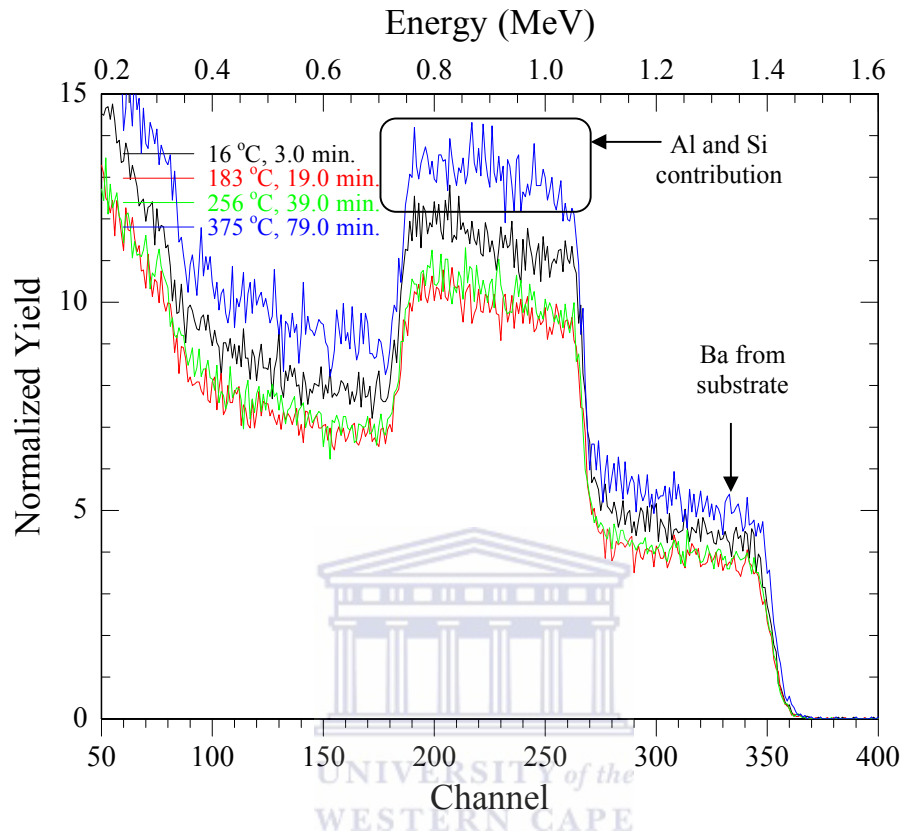
Figure 4.25 The RBS spectrometry spectra of the AICPD film annealed at elevated temperatures.

4.5.7 Hall Effect

The *AICPD* films were characterized by their electrical properties using the Hall Effect technique. The active carrier concentration of the p-doped grown films as determined from the Hall Effect measurement showed an active carrier concentration in the order of 3×10^{12} cm^{-3}. The dark conductivity of the films was determined from the procedure presented in chapter two. The dark conductivity of the films was in the range of 10^{-3} Ω^{-1}cm^{-1} for all the films. This value of dark conductivity is comparable to that of the films prepared by MIC.

Figure 4.26. The dark conductivity plot at different deposition pressures used in growth of the AICDP film. (Curve and line is a guide to the eye.)
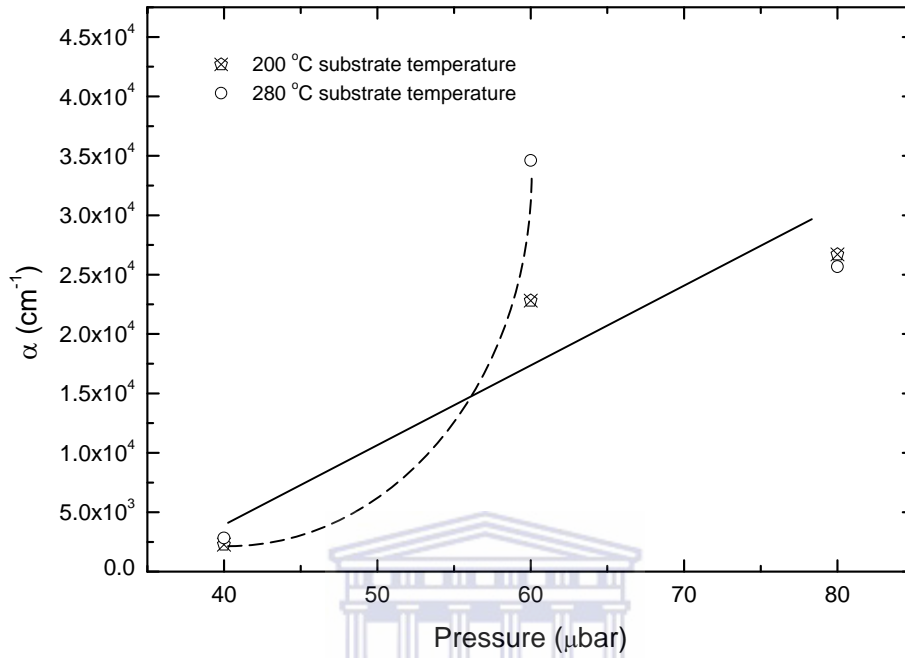
References:

[4.1] Spear, W.E. and LeComber, P.G *Solid State Co*mm. **17**, 1193 (1975).

[4.2] M.Stutzman, Handbook on semiconductors, Vol 3A, North-Holland, Amsterdam 1994.

[4.3] M. A. Bakry, Ajmed H. El-Naggar. *Thin Solid Films* **360**, 293 – 207 (2000).

[4.4] R.A. Street*, Hydrogenated amorphous silicon, Cambridge University Press* (1991).

[4.5] R.E.I. Schropp and M. Zeman, *Amorphous and microcrystalline silicon solar cell: Modeling, Materials and Device Technology*, Kluwer Academic Publisher (1998).

[4.6] B.D. Cullity. Elements of X-ray diffraction, Addison- Wisley Publishing Company, Reading, Massachusetts (1978).

[4.7] A.H. Mahan, J. Yang, S. Guha, D.L. Williamson, Mater. Res. Symp. Proc **557**, 296 (1996).

[4.8] A.H. Mahan, D.L. Williamson, T.E. Furtak, Mater. Res. Symp. Proc. **467**, 657 (1997)

[4.9] D.L. Willianson, Mater. Res. Symp. Proc. **557**, 251 (1991).

[4.10] D. Beeman, R. Tsu, M.F. Thorpe, *Physical. Review*. **B32** 874 (1985).

[4.11] Bas. B. Van Aken, C. Devilee, M. Dorenkamper, M. Geusebroek, C.R.M. Heijna. J. Loffter. W.J. Soppe. *J. of Cryst. Sol*. **354** 2392 – 2396 (2008).

[4.12] O .Nast, T Puzzer, C.T. Chou, M. Brirkholz, 16th   EPV SEC, Glasgow, UK, 2000.

[4.13] S.Gall M. Muske, I. Sieber, O.Nast, W. Fuhs, *J. Non-Cryst. Solids* **741** 299 - 302 (2002).

[4.14] J. Klein, J. Schneider, m. Muske, S. Gall, W. Fuhs, *Thin Solid Films* **451-452** 481-484 (2004).

[4.15] D. dimiva-Malinovska, O. Angelov, M. Sendova-Vassileva, M. Kamenova, J-C. Pivin, *Thin Solid Films* **451-452** 303-307 (2004).

[4.16] S.R. Herd, P. Chaudhari, M.H. Brodsky, *J. Non-Cryst. Solids* **7** 309 (1972)

[4.17] O. Nast, T. Puzzer, C.T. Chou, M. Birkholz, in; Proceesings of the 16th European Photovoltaic Solar energy Conference, Glasgow, UK, 2000

[4.18] J.B. Lee, C.H. Kim, S.Y. Kwon, D,K. Choi, *Mater. Res. Soc. Symp. Proc*. **664** A6.8.1 (2001).

References:

[4.19] S.W. Lee, Y.C. Jeon, S.K. joo, *Appl. Phys. Lett*. **66** 1671 (1995).

[4.20] S.W. Lee, S.K. Joo, *IEEE Electr. Devices Lett* **17** 160 (1996)

[4.21] C.J. Lee, J.B. J.B. Lee, Y.C. Chung, D.K. Cjoi, *Jpn. J. Appli. Phys*. **39** 6191 (2000)

[4.22] O. Nast, S. Brehme, D.H. Neuhaus, S.R. Wenham, *IEEE Trans. Electr. Devices* **46** 2062 (1996)

UNIVERSITY *of the*
WESTERN CAPE

Chapter 5

5.1 DEVICE FABRICATION

5.1.1 The n-i-p configuration

The hydrogenated amorphous silicon solar cell usually consists of an intrinsic layer sandwiched between the n-type and the p-type films. In this device configuration the intrinsic layer acts as an active layer where the photo-excited carriers are generated [5.1]. The devices fabricated for this study were grown on a pre-manufactured indium tin oxide (ITO) layer on a glass substrate. The n-type film for the cells was grown from PH_3 gas diluted in SiH_4 gas at various ratios. The intrinsic layer was deposited from pure silane gas and the p-type layer was grown using the newly developed AICPD process and this was followed by the deposition of an aluminium back contact. All these processes were done in a single HWCVD reaction chamber. Figure 5.1 shows the schematic representation of the n-i-p solar cell configuration.
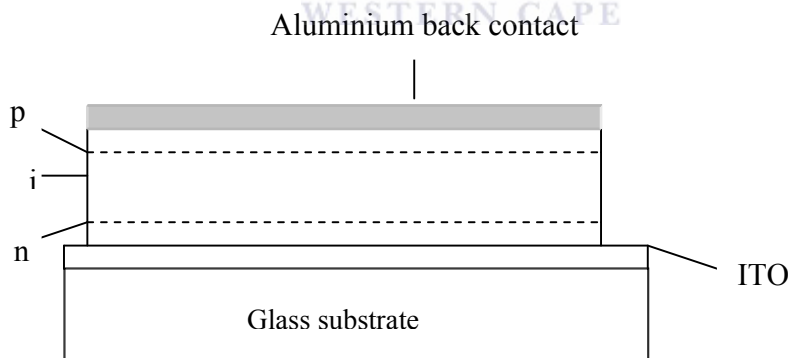
Figure 5.1 Schematic diagram of a n-i-p solar cell configuration on a glass ITO substrate.

The aluminium layer in this device functions as both the back contact and a back reflector for electromagnetic radiation. The doped layers in the devices build up the internal electric field in the intrinsic layer and this field then migrates photo-excited charged carriers in the intrinsic layer towards the doped layers in the process generating current.

In this study no band gap matching was done on the different layers for the fabrication of the solar cell, as the aim of this section will be to implement the *AICDP* grown film to manufacture a fully functional solar cell, and to prove that the *AICDP* film is operational when incorporated in a solar cell.

5.1.2 Cell fabrication

A set of various deposition conditions chosen from the analyzed results of the intrinsic film in chapter three, and the doped films in chapter four were used to manufacture the solar cell devices. The deposition conditions used for the fabrication of the devices are those that showed better optical and electrical properties relative to others. This was done to test the performance of these films in an operational solar cell.

Table 5.1 Intrinsic and n-type films analytical results recaptured.

							intrinsic
Deposition Conditions	XRD FWHM	Raman θ_b	Band gap	α at 2eV	Ref a index	FTIR H%	FTIR R*
40 µbar – 200 °C	3.90°	7.0°	1.70	22815	3.10	7.1	0.20
60 µbar – 200 °C	3.70°	6.38°	1.74	22819	3.14	6.6	0.13
80 µbar – 200 °C	3.65°	5.7°	1.75	26706	3.18	5.7	0.09
40 µbar – 280 °C	3.80°	6.8°	1.67	2200	3.12	6.0	0.18
60 µbar – 280 °C	3.75°	6.2°	1.69	34609	3.18	5.3	0.16
80 µbar – 280 °C	3.60°	5.6°	1.70	25668	3.20	5.1	0.09

						n-type
Deposition Conditions	XRD FWHM	Raman θ_b	Band gap	α at 2eV	Carrier concentration	Dark conductivity
60 µbar – 4% PH$_3$	4.0°	6.6°	1.71	22819	6.2×10^{14}	2.0×10^{-3}
60 µbar – 8% PH$_3$	4.1°	6.9°	1.68	42607	8.0×10^{15}	3.1×10^{-3}
60 µbar – 14% PH$_3$	4.2°	7.2°	1.60	46970	1.6×10^{16}	4.0×10^{-3}
80 µbar – 4% PH$_3$	4.0°	6.4°	1.72	32038	7.8×10^{15}	3.3×10^{-3}
80 µbar – 8% PH$_3$	4.1°	6.8°	1.70	36136	1.2×10^{16}	4.1×10^{-3}
80 µbar - 14% PH$_3$	4.1°	7.0°	1.68	41726	2×10^{16}	6×10^{-3}

Table 5.1 serves as a reminder of the characterization results of the intrinsic and n-type films, the highlighted parts of the table are the conditions that were used in the manufacturing of the cell. From table 5.1 a selection of the deposition conditions were chosen as listed (highlighted) in table 5.2, these values of the deposition conditions for the growth of the n-type layer, the intrinsic layer and the p-type layer were used for the solar cell fabrication.

Table 5.2 Deposition conditions used to manufacture solar cell devices.

	Devices	*Operational pressure*	*Substrate temperature*	*Filament temperature*	*Flow rate SiH₄*	*Flow rate PH₃*	*aluminium*
n-layer	Cell A	60 μbar	280 °C	1800 °C	2 sccm	48 sccm	-
	Cell B	80 μbar	280 °C	1800 °C	2 sccm	48 sccm	-
	Cell C	80 μbar	280 °C	1800 °C	4 sccm	46 sccm	-
	Cell D	80 μbar	280 °C	1800 °C	4 sccm	46 sccm	-
i-layer	Cell A	80 μbar	280 °C	1800 °C	50 sccm	-	-
	Cell B	80 μbar	280 °C	1800 °C	50 sccm	-	-
	Cell C	60 μbar	280 °C	1800 °C	50 sccm	-	-
	Cell D	40 μbar	200 °C	1800 °C	50 sccm	-	-
p-layer	Cell A	80 μbar	280 °C	1800 °C	50 sccm	-	~ 4 %
	Cell B	80 μbar	280 °C	1800 °C	50 sccm	-	~ 4 %
	Cell C	80 μbar	280 °C	1800 °C	50 sccm	-	~ 4 %
	Cell D	80 μbar	280 °C	1800 °C	50 sccm	-	~ 4%

A thickness of 30 nm was deposited for all the n-type layers during the fabrication of the solar cells in this study. The intrinsic layer thickness was set at 550 nm for all the devices, and the p-type layer was 20 nm thick. The thicknesses of the films were determined from the known deposition rate of the films that were deposited in chapter three and four. The electrical characterization of the devices was done by measuring the

open circuit voltage (V_{oc}) and short-circuit current (J_{sc}) using a sensitive digital electrometer (Keithley 1600). The V_{oc} and the J_{sc} for these fabricated devices were measured by placing the cells under 100 mW/cm^2 solar illumination. Table 5.3 lists the magnitudes of the V_{oc} and J_{sc} of these cells fabricated from their deposition conditions.

**Table 5.3** Open circuit voltage and closed circuit current of the fabricated devices.

Devices	*open circuit voltage (V_{oc})*	*short circuit current (J_{sc})*
Cell A	7.4 mV	7.1 µA
Cell B	6.4 mV	6.7 µA
Cell C	5.9 mV	5.6 µA
Cell D	4.1 mV	4.5 µA

From table 5.3 the open circuit voltages (V_{oc}) of the cells are showing improvement from cell D to cell A. A comparison between cell A and B is discussed to show the performance of the layers. From the analytical results in table 5.1, cell A n-type layer has structural properties close to that of cell B as determined from the XRD and Raman results. On the other hand the carrier concentration of cell B is greater than that of cell A as listed in table 5.1. This could be attributed to a better phosphorous incorporation in a-Si:H film under the deposition conditions used for this layer. With a higher absorption cross-section of phosphorous, the films (cell B) also exhibit an elevated absorption coefficient compared to that of the n-type layer of cell A. Using the same deposition conditions for the intrinsic layer for cell A and cell B, the cell A shows a higher V_{oc} and J_{sc} as compared to cell B. This is attributed to the higher absorption coefficient of the n-layer which is the window layer in the cell. This layer could be parasitically absorbing more photons than are needed for the generation of photo-excited charge carriers in the intrinsic layer.

The intrinsic layer of cell C and cell D were deposited in different conditions, the n-type layer and p-type layer of cells C and D on the other hand were grown from the same set of deposition conditions. When comparing the V_{oc} and the J_{sc} of these cells from table 5.3, cell C has a better V_{oc} and J_{sc} than cell D. From the experimental data in table 5.1, the intrinsic layer of cell C showed better structural and optical properties than those of cell D. Since the intrinsic layer is where the photo-excited carriers are generated, a better intrinsic layer gives a better performance in the cell.

When the 'non-optimum' deposition conditions are used to grow cells films, the V_{oc} and the J_{sc} are diminished in magnitude. The V_{oc} and the J_{sc} results of the cells in table 5.2 attest that the quality of a solar cell is directly linked to the quality of the films. The cell that is fabricated from films with superior qualities shows better performance compared to the other cells.

5.2 General conclusions
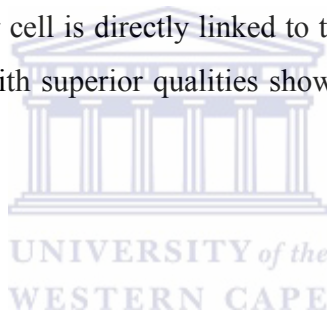
In this study we set out to develop a n-i-p solar cell by growing the p-type layer using aluminium as a dopant. This p-type layer was grown by letting the hydrogen-silicon radicals from the silane precursor gas react with evaporated aluminium. The proposal is that species reacted on their way to the heated substrate and coalesced and agglomerated on a heated substrate resulting in a film that is p-type doped crystalline.

The films that were incorporated in the solar cell device were analyzed for structural, optical and electrical properties. This was done in order to find the optimum regime for the deposition of the films for solar cell application.

The n-i-p solar cells were fabricated on pre-manufactured ITO film on glass. The n-type layers for the cells were grown using varying deposition conditions onto the ITO film. This was followed by the intrinsic layer and the p-type layer. The devices showed

photovoltaic activity as it was evident from the measured results of the V_{oc} and J_{sc} under A.M 1.5 illumination. These results were a proof that the process of *AICDP* for a p-type layer for solar cell application was successful.

The V_{oc} and the J_{sc} of the cells showed varying magnitudes depending on the film's optoelectrical characteristics, with cells that are grown at optimum conditions showing a better performance. This was evident from the comparison study between the cell A, cell B and C.

5.3 Recommendations

The performance of the cells with the p-type film as a window layer is one of the investigations that can emerge from this study. This possible study can be done by also varying the deposition conditions of the p-type layer especially to see effects of the aluminium concentration on the performance of the cell.

WESTERN CAPE
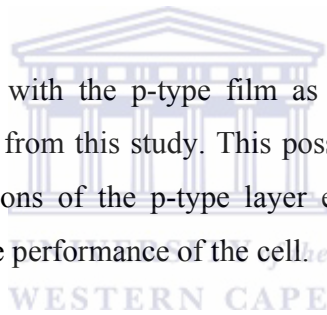
A study on the structural effect and electrical behaviour of the *AICDP* film can be conducted, to test the effect that hydrogen dilution will have on the growth of the p-type film.

The author also recommends a further study on the nature of the reaction between the, aluminium atoms and the silicon hydride in the gas phase, and which silicon hydrides species are better suited for the promotion of the p-doping reaction.

Reference:

[1] K.F. Feenstra, *Hot-wire chemical vapour deposition of amorphous silicon and the application in solar cells*, Ph.D thesis, Utrecht University , 1998.